© 2022. Published by The Company of Biologists Ltd | Development (2022) 149, dev199987. doi:10.1242/dev.199987

RESEARCH ARTICLE

Traip controls mushroom body size by suppressing mitotic defects

Ryan S. O'Neill* and Nasser M. Rusan*

ABSTRACT

Microcephaly is a failure to develop proper brain size and neuron number. Mutations in diverse genes are linked to microcephaly, including several with DNA damage repair (DDR) functions; however, it is not well understood how these DDR gene mutations limit brain size. One such gene is *TRAIP*, which has multiple functions in DDR. We characterized the *Drosophila TRAIP* homolog *nopo*, hereafter *traip*, and found that *traip* mutants (*traip*$^{-}$) have a brain-specific defect in the mushroom body (MB). *traip*$^{-}$ MBs were smaller and contained fewer neurons, but no neurodegeneration, consistent with human primary microcephaly. Reduced neuron numbers in *traip*$^{-}$ were explained by premature loss of MB neuroblasts (MB-NBs), in part via caspase-dependent cell death. Many *traip*$^{-}$ MB-NBs had prominent chromosome bridges in anaphase, along with polyploidy, aneuploidy or micronuclei. Traip localization during mitosis is sufficient for MB development, suggesting that Traip can repair chromosome bridges during mitosis if necessary. Our results suggest that proper brain size is ensured by the recently described role for TRAIP in unloading stalled replication forks in mitosis, which suppresses DNA bridges and premature neural stem cell loss to promote proper neuron number.

KEY WORDS: Brain development, DNA damage, *Drosophila*, Microcephaly, Traip

INTRODUCTION

Microcephaly is a developmental growth disorder characterized by reduced cerebral cortex size and neuron number. Mutations in about 40 genes are linked to microcephaly, ranging from microcephaly, primary, hereditary (MCPH; Jayaraman et al., 2018), in which only brain size is reduced, to more severe forms, such as Seckel syndrome (SCKL), in which both brain and body are reduced in size (Khetarpal et al., 2016). Most microcephaly disorders are linked to mutations in genes with one of two functions: centrosome and mitotic spindle functions, or DNA damage repair (DDR). Mutations in centrosome/mitotic spindle genes are thought to disrupt spindle structure and orientation, leading to defects in chromosome segregation or cell cycle progression and, ultimately, neural progenitor cell (NPC) loss through premature differentiation or cell death (reviewed by Nano and Basto, 2017). Mutations in DDR genes are thought to increase DNA damage, activate checkpoint signaling and lead to increased genome instability, cell cycle lengthening and the ultimate loss of NPCs (reviewed by Bianchi et al., 2018). However, most microcephaly genes have not been directly studied in the context of brain development and the cellular etiology of microcephaly has been inferred from studies in non-neuronal contexts. Thus, we aimed to study the microcephaly gene *TRAIP* in an animal to reveal the etiological mechanisms of disease.

TRAIP encodes a RING domain E3 ubiquitin ligase that localizes to the nucleus and functions in DDR. In humans, mutations in *TRAIP* cause SCKL with severe microcephaly and reduced body size (Harley et al., 2016). Cultured fibroblasts from individuals with *TRAIP* mutations have an elongated cell cycle and impaired DNA repair, suggesting that *TRAIP* mutations cause microcephaly as a result of reduced proliferation, premature differentiation, and apoptosis of NPCs (Harley et al., 2016). A mouse *Traip* mutant is early embryonic lethal (Park et al., 2007) and *Drosophila* mutants for the *TRAIP* ortholog *nopo* (herein called *traip*) are maternal-effect lethal (homozygous null mothers lay eggs that arrest in the first few embryonic cell cycles; Merkle et al., 2009), whereas null mutant *Caenorhabditis elegans* are viable (Sonneville et al., 2019). No studies of *TRAIP* function in developing brains have been published.

TRAIP has several functions related to DDR (reviewed by Wu et al., 2020). TRAIP localizes to double-strand breaks, where it recruits other factors and promotes H2B monoubiquitylation to stimulate repair (Han et al., 2019; Soo Lee et al., 2016). TRAIP also localizes to stressed replication forks (Feng et al., 2016; Hoffmann et al., 2016) where it removes DNA-protein crosslinks (Larsen et al., 2019) and regulates the choice between NEIL3 or FANC/BRCA-mediated repair pathways (Wu et al., 2019). In addition to these interphase DDR functions, TRAIP also promotes sister chromatid separation during mitosis. A cell entering mitosis may have under-replicated sister chromatids (URSCs), which contain loci that failed to complete replication during interphase, and these URSCs must be resolved to prevent DNA bridges during anaphase. TRAIP initiates the resolution of URSCs by ubiquitylating the MCM7 subunit of CMG helicase at mitotic entry, thus triggering fork unloading and allowing sister chromatid resolution via mitotic DNA repair synthesis (Deng et al., 2019; Priego Moreno et al., 2019; Sonneville et al., 2019; Villa et al., 2021).

However, most previous studies on TRAIP function were performed in cell culture, *Xenopus* egg extracts, and the early embryos of *Drosophila* and *C. elegans*, and thus it is unclear which TRAIP functions are essential for neurogenesis. In this study, we take advantage of the well-characterized brain structure and genetic tractability of *Drosophila* to establish a model of *traip* mutant microcephaly. In this context, Traip functions in NSCs during mitosis to suppress DNA bridges and prevent premature NPC loss, pointing to a role in URSC resolution as crucial for proper brain size.

RESULTS

traip is required for proper mushroom body development

We generated a new full coding sequence deletion of *traip* using CRISPR (*traip*$^{\Delta}$). We use *traip*$^{-}$ to refer to *traip*$^{\Delta}$ in combination

Cell and Developmental Biology Center, National Heart Lung and Blood Institute, National Institutes of Health, Bethesda, MD 20892, USA.

*Authors for correspondence (oneillrs@nih.gov; nasser@nih.gov)

R.S.O., 0000-0001-8673-9217; N.M.R., 0000-0002-4194-1072

Handling Editor: Irene Miguel-Aliaga
Received 7 July 2021; Accepted 28 February 2022

Development (2022) 149, dev199987. doi:10.1242/dev.199987

with either the previously described null allele *traip*^{Exc142} (Merkle et al., 2009) or the deficiency *Df(2R)Exel7153* (Parks et al., 2004), as both allelic combinations showed identical brain phenotypes.

To test whether *traip* controls brain size, we used µ-computed tomography (µ-CT; Schoborg et al., 2019) to compare control and *traip*$^{-}$ adult brains using normalized volumetric analysis (Fig. 1A). Although optic lobes were not different (Fig. 1B), *traip*$^{-}$ central brain volume was slightly reduced, and this reduction was rescued by a ubiquitously expressed GFP-tagged *traip* transgene (*ubi-GFP::traip*; Fig. 1C). This suggested that *traip* is required for fully proper brain development.

To determine whether any specific brain subregion was disrupted, we examined neuropil (Cadherin-N; CadN) and axon tracts (Neuroglian; Nrg) in *traip*$^{-}$ brains. All brain regions appeared qualitatively similar (Fig. S1A), except for a 100% penetrant size and structure defect in *traip*$^{-}$ mushroom bodies (MBs), a pair of neuropils that mediate higher-order functions in the insect brain (Fig. 1D; Heisenberg, 2003; Modi et al., 2020). In *Drosophila*, each MB arises from four neuroblasts (MB-NBs), which divide continuously from embryonic development through late pupal stages to produce roughly 2500 Kenyon cells (KCs) per hemisphere (Fig. 1E). These KCs are positioned on the posterior dorsal side of the brain and project axons in a stereotypic, bifurcated pattern to form the γ (first born), α′/β′, and α/β (last born) lobes of the MB (Fig. 1D).

The MBs of *traip*$^{-}$ adult brains were misshapen and reduced in size (Fig. 1G), with additional axon-related defects: 50% with axon tracts exiting the lobes (0% in controls), 93% with lobes fused at the midline (14% in controls), and 29% missing α or β lobes (0% in controls). *traip*$^{-}$ α/β lobe volume, identified by FasII (Fas2) staining, was reduced by 70% (Fig. 1H,I), and *traip*$^{-}$ full MB volume, identified by mCD8::GFP expression driven in KCs by *OK107-GAL4*, was reduced by 37% (Fig. S1B,C). The more severe size reduction of the last-born, FasII-positive α/β lobes indicates that the *traip*$^{-}$ MB defect progressively accumulates through development. Cross-sectional area was also reduced in FasII-positive α lobes by 84% (Fig. 1J) and *OK107-GAL4*>mCD8::GFP α′/α lobes by 54% (Fig. S1D).

MB lobe size reduction was consistent across all *traip* null mutant combinations (Fig. S1E), whereas hypomorphic mutants (Merkle et al., 2009) had wild-type MB lobe size (Fig. S1E,F). MB lobe size was rescued by ubiquitously expressing GFP::Traip (Fig. S1G,H), and importantly, by specifically expressing GFP::Traip in the MB-NBs and KCs via *OK107-GAL4* (Fig. 1I-K). Thus, MB lobe size reduction is linked to cell-autonomous loss of Traip function in the MB-NBs and/or KCs.

Reduced *traip*$^{-}$ MB lobe size suggests reduced KC number. We used machine learning to count KCs with *OK107-GAL4*>NLS::mCherry (Fig. 1L). Each *traip*$^{-}$ hemisphere contained an average of 699 KCs, a 62% reduction compared with controls, which had 1852 KCs (Fig. 1M). KC number in *traip*$^{-}$ was rescued by *OK107-GAL4>UAS-GFP::traip* (Fig. 1L,M). Regression analyses showed a significant linear correlation between KC number and both MB volumes (Fig. S2I) and cross-sectional areas (Fig. S2J). Having shown that α lobe cross-sectional area measurement was a suitable proxy for KC number, we used this measurement for the remainder of this study.

traip is required in MB-NBs during development

To determine whether the *traip*$^{-}$ MB lobe defects were developmental (primary microcephaly-like) or neurodegenerative (secondary microcephaly-like; Passemard et al., 2013), we investigated pre-adult stages (Fig. 2A). In the third instar larval stage, when only γ lobes are present, *traip*$^{-}$ MB lobe size was not significantly reduced compared with controls (Fig. 2B). However, during pupal stages there was a significant reduction in MB lobe size of *traip*$^{-}$ compared with controls (Fig. 2C). Note that the large reduction in MB cross-sectional area between larval and 24 h after pupal formation (APF) stages is due to extensive developmental remodeling of the short, thick larval γ lobes during metamorphosis, which are replaced by longer, thinner α lobes during the early pupal stages (Lee et al., 1999). Thus, *traip*$^{-}$ exhibits primary microcephaly-like defects, as MB lobe size reduction arises during development.

We investigated the possibility of neurodegeneration by comparing MBs of 3-day-old and 50-day-old adults (Fig. 2D). MB lobe size increased slightly with age in controls (Fig. 2E), reflecting neuropil reorganization in response to life experience (Heisenberg et al., 1995). In contrast, *traip*$^{-}$ MBs neither grew nor shrunk with age (Fig. 2E). Thus, *traip*$^{-}$ MB lobe size reduction is not neurodegenerative and does not reflect secondary microcephaly.

We hypothesized that the reduced KC number and MB lobe size observed in *traip*$^{-}$ could arise in two ways: (1) a defect in the highly mitotic MB-NBs resulting in fewer KCs born, and (2) a defect in the differentiated KCs resulting in cell death. We began to explore which cell types express Traip, using CRISPR to knock in *mNeonGreen* at the endogenous *traip* locus (*mNG::traip*), which resulted in a fly line with wild-type MB morphology (Fig. S2A). mNG::Traip was expressed in all third instar larval central brain neuroblasts (CB-NBs), which include the MB-NBs (Fig. 3A). In addition, mNG::Traip expression persisted in the ganglion mother cells (GMCs) and their immediate daughter neurons (Fig. 3B). However, mNG::Traip was absent from regions of mature neurons in larval brains (Fig. 3A), and was not detectable in adult brain neurons (Fig. S2B). These data suggest that Traip primarily functions in proliferating brain cells.

To determine which cell types require Traip function, we used cell type-specific expression of GFP::Traip in attempt to rescue *traip*$^{-}$ MB lobe size. First, we used *wor-GAL4* to drive *UAS-GFP::traip* in NBs, which rescued MB lobe size (Fig. 3C,D). However, this did not fully exclude a role for Traip in neurons, as *wor-GAL4*>GFP::Traip was also found in GMCs and newly born neurons (Fig. S2C). We next tried expressing GFP::Traip in post-mitotic neurons using *elav-GAL4*, but discovered strong expression in the neuroblasts (NBs) and GMCs (Fig. S2D). Finally, we used *nSyb-GAL4* to drive GFP::Traip expression in mature neurons (Fig. S2E), which failed to rescue MB lobe size (Fig. 3E,F). Thus, Traip function in neurons alone is insufficient to prevent microcephaly. We conclude that the primary function for Traip is in proliferating brain cells (NBs and GMCs), although we could not fully rule out the possibility that undetectable levels of Traip also function in post-mitotic neurons.

traip mutant MB-NBs are lost via caspase-dependent cell death

We next hypothesized that *traip*$^{-}$ reduction in KC number and MB lobe size is due to premature loss of MB-NBs. The KCs of each MB arise from four MB-NBs that are easily identifiable at 24 h APF, as nearly all other NBs have been lost by this stage (Ito and Hotta, 1992; Truman and Bate, 1988). Controls maintained four MB-NBs throughout pupal development (Fig. 4A,B). In contrast, *traip*$^{-}$ progressively lost their MB-NBs, with an average 2.2 MB-NBs per hemisphere at 24 h APF decreasing to 0.9 by 72 h APF, and this loss was rescued by *OK107-GAL4>UAS-GFP::traip* (Fig. 4A,B).

Development (2022) 149, dev199987. doi:10.1242/dev.199987

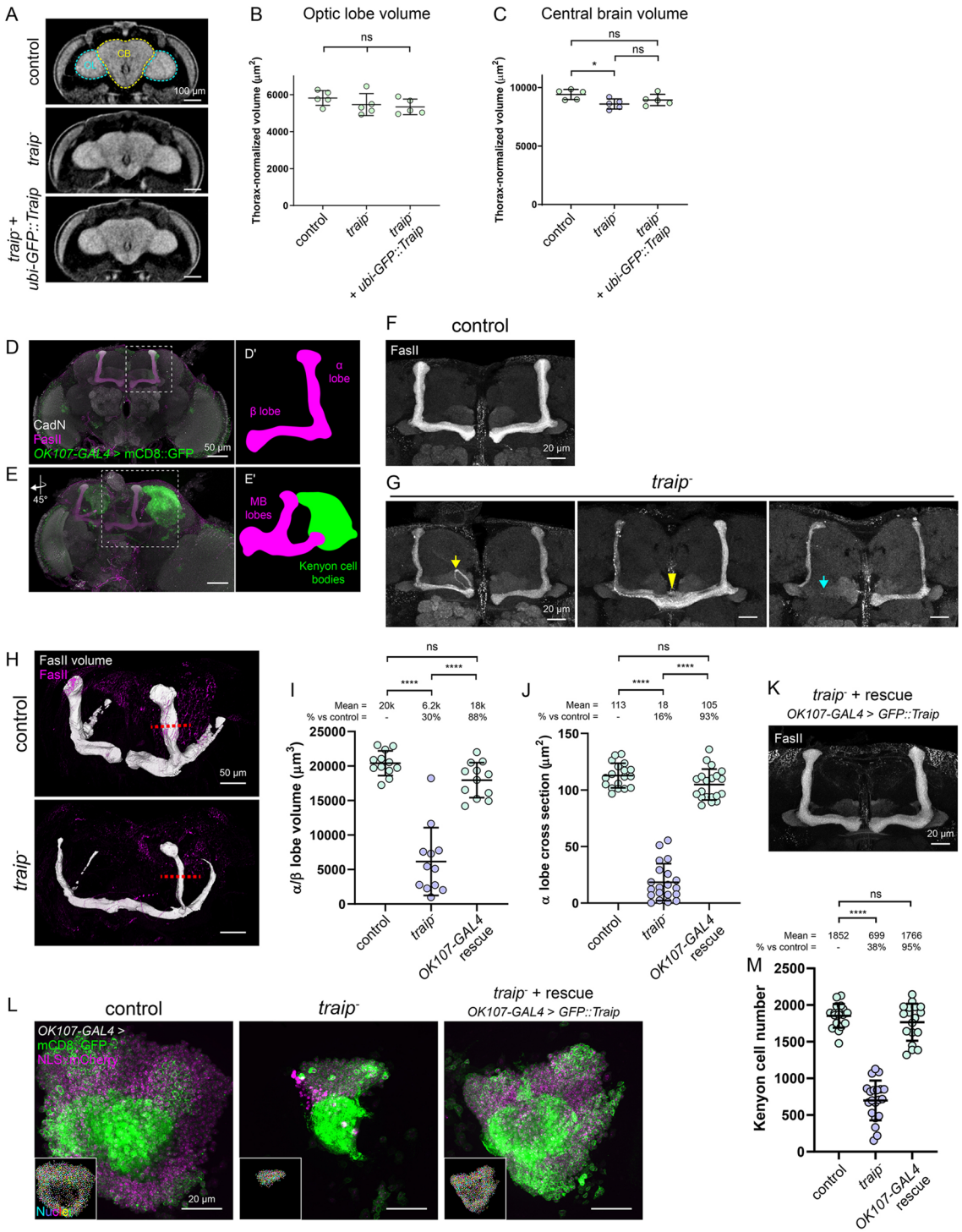

Fig. 1. *traip* is required for proper MB structure. (A) µ-CT tomograms of control, *traip*⁻ and *traip*⁻+*ubi-GFP::traip* adult brains. Optic lobes (OL) and central brain (CB) are highlighted on the control. (B) Thorax-normalized optic lobe volumes. *n*=5 brains. (C) Thorax-normalized central brain volumes. *n*=5 brains; **P*=0.034. (D) Maximum projection of an adult brain stained for FasII (α/β lobes, magenta; schematic in D′) and CadN (neuropil, white) and labeled with *OK107-GAL4*>mCD8::GFP (green). Dashed box indicates the region schematized in D′. (E) Oblique full brain volume projection stained for FasII and CadN, and labeled with *OK107-GAL4*>mCD8::GFP, showing KC bodies on the ventral posterior side projecting axons anteriorly to form the MB lobes (schematic in E′). (F) Control MBs stained for FasII with stereotypical L-shaped α/β lobes. (G) *traip*⁻ MBs with reduced size, misguided axon tracts (yellow arrow, 50% *traip*⁻ versus 0% control), midline fused MBs (yellow arrowhead, 93% *traip*⁻ versus 14% control), and missing α or β lobes (cyan arrow, 29% *traip*⁻ versus 0% control). (H) Control and *traip*⁻ α/β lobe volumes (white) segmented from FasII staining (magenta). Red dashed lines show the position of cross-section measurements. (I) α/β lobe volume measurements. *n*≥12 MBs. (J) α lobe cross-section measurements. *n*≥18 MBs. (K) MBs from *traip*⁻+*OK107-GAL4>GFP::traip* rescue. (L) Machine-learning segmentation of KCs. *OK107-GAL4*>mCD8::GFP (green)+NLS::mCherry (magenta) were used for KC nuclei segmentation and counting (multicolor, inset) of control, *traip*⁻ and *traip*⁻+*OK107-GAL4>GFP::traip* rescue. (M) KC numbers per hemisphere. *n*≥16 hemispheres. In all graphs, bars are mean±s.d. Ordinary one-way ANOVA (B,C,I,J,M) was used to determine significance. ns, not significant; *****P*<0.0001. Scale bars: 100 µm (A); 50 µm (D,E,H); 20 µm (F,G,K,L).

Development (2022) 149, dev199987. doi:10.1242/dev.199987

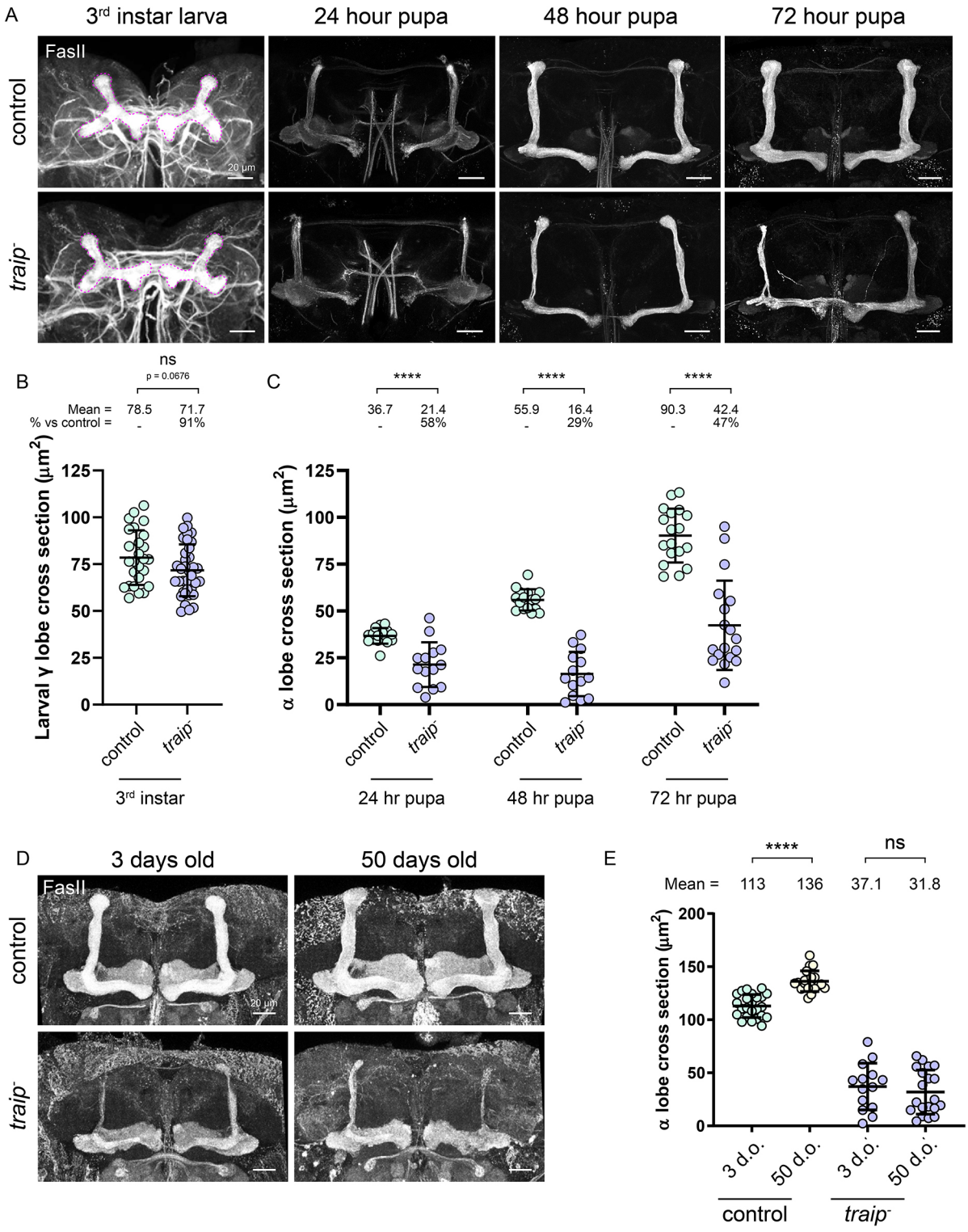

Fig. 2. *traip* is required for MB development. (A) Control (top) and *traip*$^{-}$ (bottom) MBs from (left to right) third instar larvae, 24 h APF, 48 h APF and 72 h APF pupae stained for FasII. Third instar larval MBs are highlighted in magenta; note that in the larval stage, FasII labels γ lobes, and α/β lobes are yet to be born. (B) Third instar larval γ lobe cross-section measurements of control and *traip*$^{-}$. $n \geq 14$ MBs. (C) α lobe cross-section measurements of control and *traip*$^{-}$ pupal stages. $n \geq 14$ MBs. (D) Control (top) and *traip*$^{-}$ (bottom) MBs from 3-day-old adults (left) and 50-day-old adults (right) stained for FasII. (E) α lobe cross-section measurements show that control MBs increase in size with age, whereas *traip*$^{-}$ MBs do not change. $n \geq 14$ MBs. Two-tailed *t*-test was used to determine significance. ns, not significant; ****$P<0.0001$. Scale bars: 20 µm.

To explore the role of caspase-dependent cell death in MB-NB loss, we used *Df(3L)H99*, which deletes four pro-apoptotic genes (*grim*, *rpr*, *hid* and *skl*; Abbott and Lengyel, 1991). MB-NB loss was suppressed in *traip*$^{-}$ with *Df(3L)H99* compared with *traip*$^{-}$ alone at 24 h APF (3.1 versus 2.2; Fig. 4A,B), although this effect was not observed in later stages. *Df(3L)H99* also improved *traip*$^{-}$

Development (2022) 149, dev199987. doi:10.1242/dev.199987

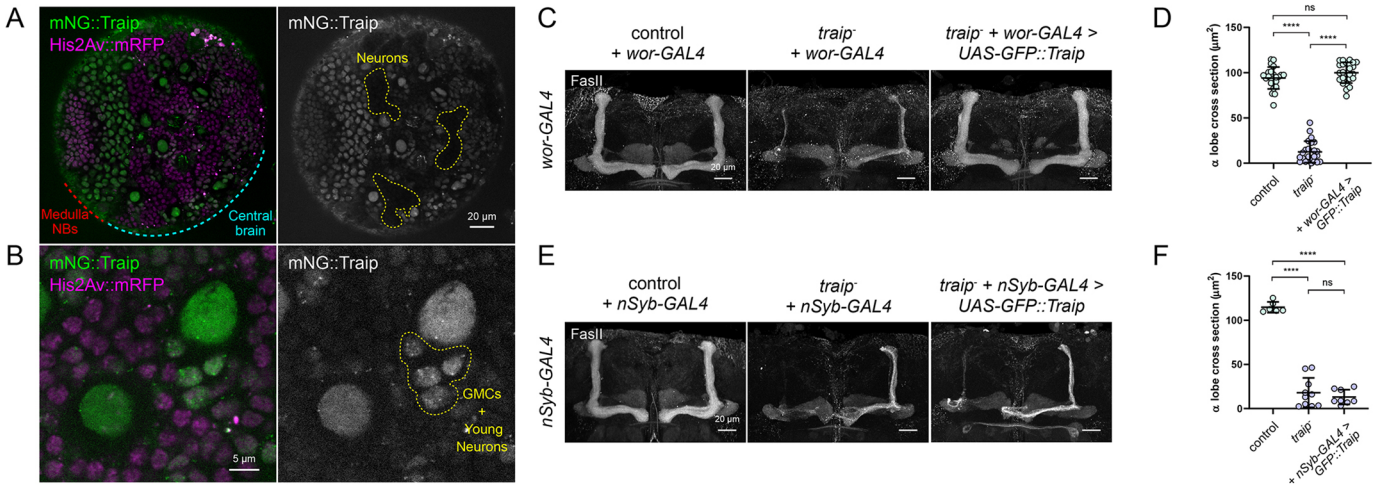

Fig. 3. *traip* is required in NBs. (A) Endogenously tagged mNG::Traip (green, gray) and His2Av::mRFP (magenta) in the third instar larval brain. mNG::Traip is highly expressed in the proliferating cells of the medulla (red zone) and central brain regions (cyan zone), but is absent from areas dominated by neurons (yellow outlines). (B) High-resolution imaging of mNG::Traip localized to the nuclei of interphase CB-NBs, and persisting in daughter GMCs and young neurons (yellow outline). (C) MBs from control, *traip*$^{-}$ and *UAS-GFP::traip* rescue, all with *wor-GAL4*, stained for FasII. (D) α lobe cross-section measurements show that *traip*$^{-}$*+wor-GAL4>GFP::traip* rescue MBs are similar in size to wild-type MBs. $n \geq 22$ MBs. (E) MBs from control, *traip*$^{-}$ and *UAS-GFP::traip* rescue, all with *nSyb-GAL4*, stained for FasII. (F) α lobe cross-section measurements show that *traip*$^{-}$*+nSyb-GAL4>GFP::traip* have reduced MB size. $n \geq 6$ MBs. Ordinary one-way ANOVA was used to determine significance. ns, not significant; ****$P<0.0001$. Scale bars: 20 µm (A,C,E); 5 µm (B).

MB lobe size more than 2-fold (Fig. 4D,E) and improved KC number by 1.4-fold (Fig. 4F,G). Because *Df(3L)H99* deletes other genes, we used RNAi against the effector caspase *Drice*, which improved *traip*$^{-}$ MB lobe size by 1.6-fold (Fig. 4E,H). We also stained control and *traip*$^{-}$ for cleaved caspase Dcp-1 at the 24 h APF stage, observing one actively dying MB-NB in *traip*$^{-}$ (Fig. 4I,J). Both controls and *traip*$^{-}$ had similar numbers of Dcp-1-positive KCs or GMCs per hemisphere (Fig. 4K). However, controlling for the total number of KCs suggested that *traip*$^{-}$ had a significantly higher proportion of actively dying KCs and/or GMCs compared with controls (Fig. 4L). Together, these data support a model in which Traip prevents premature loss of MB-NBs (and possibly KCs and/or GMCs), and that in the absence of Traip these cells are lost in part via caspase-dependent cell death.

traip suppresses chromosome bridges during anaphase

After noticing abnormal nuclei while scoring *traip*$^{-}$ MB-NB number, we characterized nuclear phenotypes in 24 h APF MB-NBs to gain insight into defects potentially upstream of MB-NB loss. Control MB-NBs had nuclei with relatively smooth, spherical nuclear lamina morphology and no other defects (100%; Fig. 5A). In contrast, some *traip*$^{-}$ MB-NBs appeared apoptotic, with abnormally condensed DAPI staining (11%; Fig. 5B), and others frequently had nuclear defects, including irregular, crenellated nuclear lamina morphology (12%; Fig. 5C), micronuclei (11%; Fig. 5D), multiple nuclei (9%; Fig. 5E) or extremely large nuclei suggestive of polyploidy (9%; Fig. 5F). These *traip*$^{-}$ phenotypes were rescued by *OK107-GAL4>UAS-GFP::traip* (Fig. 5G).

As these nuclear defects could arise during mitosis, we used high-resolution live fluorescence microscopy to analyze mitotic dynamics of third instar larval CB-NBs. We chose to image general CB-NBs because of technical constraints that limited the ability to image MB-NBs properly at high resolution. Unlike control NBs (Fig. 5H, Movie 1), 26% of *traip*$^{-}$ NBs had prominent chromosome bridges, where sister chromatids appeared attached and did not effectively separate at anaphase onset, but rather became stretched across the midzone through anaphase before eventually separating (Fig. 5I,J, Movies 2,3). Furthermore, *traip*$^{-}$ larval brains often had cells with abnormally large nuclei (Fig. S3A), reminiscent of the suspected polyploid cells seen in *traip*$^{-}$ pupal brains (Fig. 5E). We did not observe any other obvious mitotic defects in *traip*$^{-}$ NBs. Expressing GFP::Traip via *wor-GAL4* rescued these mitotic bridge defects (Fig. 5K, Movie 4). We reasoned that *traip*$^{-}$ mitotic DNA bridges could block cytokinesis, resulting in multiple nuclei or polyploidy, or else lead to chromosome breakage, resulting in micronuclei.

We also used live imaging to explore potential mitotic delays in *traip*$^{-}$ NBs. Measuring the time from anaphase onset to the moment of complete furrow constriction showed no difference between controls, *traip*$^{-}$ and *wor-GAL4>UAS-GFP::traip* rescues, and the presence or absence of DNA bridges in *traip*$^{-}$ NBs did not affect mitotic timing (Fig. 5L). However, we were unable to identify abscission definitively, and in one case a *traip*$^{-}$ NB with a DNA bridge experienced a period of disrupted cortical activity (Movie 3), suggesting a possible delay in abscission. We also found no difference in the duration from prophase onset to complete furrow constriction for CB-NBs (Fig. S3B). In fixed larval brains, the mitotic index of control and *traip*$^{-}$ CB-NBs were similar (Fig. S3C). In 24 h APF brains, the mitotic index of *traip*$^{-}$ MB-NBs was lower than controls (20% *traip*$^{-}$ versus 35% controls); however, when MB-NBs with nuclear defects (Fig. 5B-F) were excluded from this analysis, the mitotic index of phenotypically normal *traip*$^{-}$ MB-NBs was not different from controls (32% *traip*$^{-}$ versus 35% controls; Fig. S3D). Thus, the reduced mitotic index of *traip*$^{-}$ MB-NBs could be explained by an inability of polyploid, multinucleate and apoptotic cells to enter mitosis rather than a function for Traip in directly controlling mitotic or cell cycle timing.

We also found evidence suggesting persistent aneuploidy in *traip*$^{-}$ MB-NBs. Control pupae expressing both mCD8::GFP and NLS::mCherry via *OK107-GAL4* had similar fluorescence levels across the field of mature KCs (Fig. 5M). In contrast, *traip*$^{-}$ pupae often contained one or more clusters of KCs that had either double the signal or no signal for the GFP or mCherry marker (Fig. 5N). These aberrant KC clusters were reminiscent of clonal cell clusters, suggesting that their MB-NB progenitors became aneuploid, either

Development (2022) 149, dev199987. doi:10.1242/dev.199987

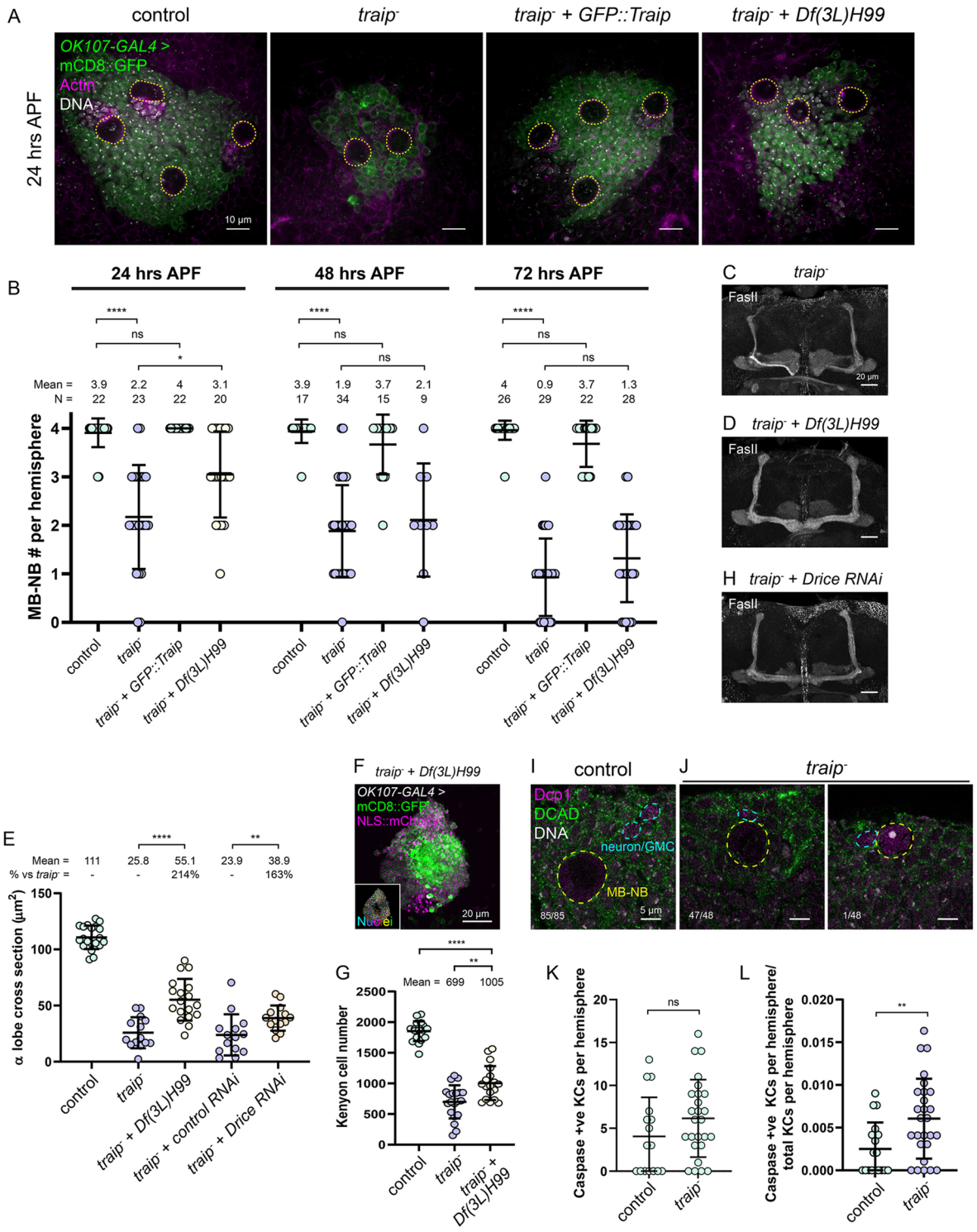

Fig. 4. *traip* suppresses MB-NB cell death. (A) Fields of KCs and MB-NBs labeled with *OK107-GAL4*>mCD8::GFP (green), phalloidin (magenta) and DNA (gray) from (left to right) control, *traip*$^{-}$, *traip*$^{-}$+*OK107-GAL4>GFP::traip* rescue and *traip*$^{-}$+*Df(3L)H99* 24 h APF pupae. NBs are highlighted in yellow. Scale bars: 10 µm. (B) MB-NB number per brain hemisphere for control, *traip*$^{-}$, *traip*$^{-}$+*GFP::traip* rescue and *traip*$^{-}$+*Df(3L)H99* at 24, 48 and 72 h APF pupal stages. **P*=0.0195. *n* is reported above each column. (C,D,H) Maximum projections of adult MBs stained for FasII. Genotypes are: *traip*$^{-}$ (C); *traip*$^{-}$+*Df(3L)H99* (D); *traip*$^{-}$+*OK107-GAL4>Drice* RNAi (H). Scale bars: 20 µm. (E) α lobe cross-section measurements of control, *traip*$^{-}$, *traip*$^{-}$+*Df(3L)H99*, *traip*$^{-}$+control RNAi and *traip*$^{-}$+*Drice* RNAi. ***P*=0.0090. $n \geq 14$ MBs. (F) *OK107-GAL4*>mCD8::GFP (green)+NLS::mCherry (magenta) were used for KC nuclei segmentation and counting (multicolor, inset) of *traip*$^{-}$+*Df(3L)H99*. (G) KC numbers per hemisphere. KCs are increased by 144% in *traip*$^{-}$+*Df(3L)H99* compared with *traip*$^{-}$. Control and *traip*$^{-}$ reproduced from Fig. 1. $n \geq 16$ hemispheres. (I,J) MB-NBs (yellow dashed lines) and neurons/GMCs of control and *traip*$^{-}$ 24 h APF stained for Dcp-1 (magenta), DCAD (Shotgun; green) and DNA (gray). For controls, 85/85 MB-NBs were Dcp-1 negative. For *traip*$^{-}$, 1/48 MB-NBs assayed was Dcp-1 positive (right panel). In both controls and *traip*$^{-}$, some Dcp-1-positive neurons or GMCs were also observed (cyan dashed lines). (K) Quantification of the absolute number of Dcp-1-positive KCs or GMCs per hemisphere in control and *traip*$^{-}$. (L) Quantification of the number of Dcp-1-positive KCs and GMCs divided by the total number of neurons and GMCs per hemisphere. ***P*=0.0071. Ordinary one-way ANOVA (B,E,G) and unpaired *t*-test (K,L) were used to determine significance. ns, not significant; *****P*<0.0001.

Development (2022) 149, dev199987. doi:10.1242/dev.199987

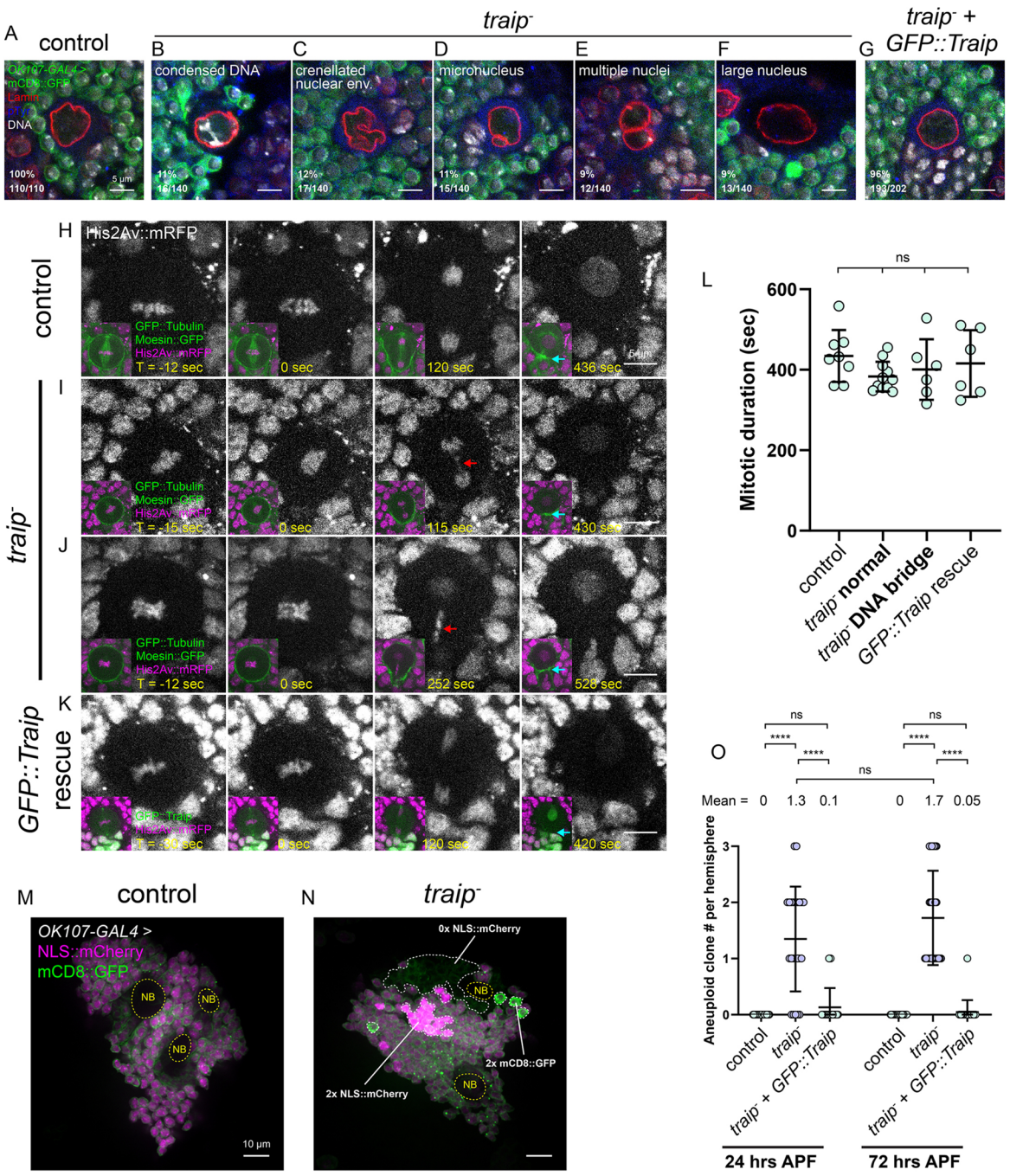

Fig. 5. *traip* suppresses multinuclear phenotypes and mitotic DNA bridges. (A-F) MB-NBs from 24 h APF pupal brains labeled with *OK107-GAL4*>mCD8::GFP (green) and stained for Lamin (red), DNA (gray) and phospho-Tyrosine (blue). (A) All (110/110) control MB-NBs have relatively smooth, spherical nuclear laminar morphology and no additional nuclear defects; (B) 11% (16/140) of *traip*$^{-}$ 24 h APF MB-NBs appeared apoptotic, with abnormally condensed DAPI staining; (C) 12% (17/140) of *traip*$^{-}$ MB-NBs have irregular, crenellated nuclear envelope morphology; (E) 11% (15/140) of *traip*$^{-}$ MB-NBs have micronuclei; (E) 9% (12/140) of *traip*$^{-}$ MB-NBs have multiple nuclei; (F) 9% (13/140) of *traip*$^{-}$ MB-NBs appeared polyploid, with abnormally large nuclei. (G) Most MB-NBs from *traip*$^{-}$*+OK107-GAL4>GFP::traip* rescues have wild-type nuclear envelope morphology (96%, 193/202), and 4% (9/202) had crenellated nuclear envelope morphology. (H) Control third instar larval CB-NBs expressing His2Av::mRFP (gray, magenta in inset) and both GFP::Tubulin and Moesin::GFP (green in inset). The second panel shows anaphase onset (T=0), and the fourth panel shows the moment of complete furrow constriction (cyan arrows). *n*=10 NBs. See also Movie 1. (I,J) 26% (5/19) of *traip*$^{-}$ CB-NBs form chromosome bridges during anaphase. Red arrows point to the chromosome bridge stretched out during anaphase. I shows a *traip*$^{-}$ NB that is otherwise normal except for the chromosome bridge (see also Movie 2). J shows a *traip*$^{-}$ NB with a prominent bridge and abnormal cortical activity (see also Movie 3). (K) Time from anaphase onset to complete furrow constriction of CB-NBs for control, *traip*$^{-}$ either with or without DNA bridges, and *traip*$^{-}$*+wor-GAL4>UAS-GFP::traip* rescue. Ordinary one-way ANOVA was used to test significance. (L) *wor-GAL4>UAS-GFP::traip* fully rescues *traip*$^{-}$ NB mitotic chromosome bridging (10/10). (M) Control 24 h APF pupae expressing *OK107-GAL4*>NLS::mCherry+mCD8::GFP show uniform fluorescence levels of both markers across the field of KCs, except for NBs (yellow outlines) and their immediate daughters, which have reduced fluorescence. (N) *traip*$^{-}$ pupae contain patches of presumably aneuploid KCs with either double or no fluorescence for one or both markers (white outlines). (O) Number of aneuploid KC clones per brain hemisphere in control, *traip*$^{-}$ and *traip*$^{-}$*+OK107-GAL4>GFP::traip* rescue at 24 and 72 h APF. Kruskal–Wallis test was used to determine significance. ns, not significant; ****P<0.0001. $n\geq$22 hemispheres. Scale bars: 5 µm (A-K); 10 µm (M,N).

Development (2022) 149, dev199987. doi:10.1242/dev.199987

losing or gaining a copy of one transgene, and then continued generating daughter cells. These clones were never observed in controls, whereas *traip*$^{-}$ brains had an average of 1.3 clones per hemisphere at 24 h and 1.7 clones per hemisphere at 72 h APF (Fig. 5O). The average number of KCs per clone in *traip*$^{-}$ brains increased from 15 at 24 h to 37 at 72 h APF (Fig. S3E), with some clones containing hundreds of KCs. *OK107-GAL4>UAS-GFP::traip* suppressed clone formation (Fig. 5L). Reasoning that these clones could arise via either whole-chromosome mis-segregation or through chromosome breakage and partial mis-segregation, we stained for γH2Av to identify double-stranded DNA breaks in 24 h APF MB-NBs. Whereas controls (Fig. S3F) and most *traip*$^{-}$ (Fig. S3G) MB-NBs had few γH2Av puncta, a small subset of *traip*$^{-}$ MB-NBs had extremely elevated γH2Av puncta (Fig. S3H,I). These data are consistent with *traip*$^{-}$ mitotic DNA bridges leading to aneuploid MB-NBs, which often continue producing daughters before eventually being lost.

traip functions to resolve URSCs

TRAIP has a known role in resolving URSCs at mitotic onset (Deng et al., 2019; Priego Moreno et al., 2019; Sonneville et al., 2019), and URSCs are predicted to form a special class of mitotic DNA bridges called ultrafine DNA bridges (UFBs; Liu et al., 2014). Human FANCD2 localizes as puncta at the points where UFBs connect with sister chromatids (Naim and Rosselli, 2009), and although FancD2 localization has not been well-characterized in *Drosophila*, there is precedence for invisible DNA tethers in *Drosophila* cells (Royou et al., 2010). Thus, to test for UFBs we generated transgenes encoding fluorescently tagged FancD2. We found that mNG::FancD2 puncta localized to mitotic DNA bridges in many *traip*$^{-}$ NBs (7/12; Fig. 6B), in addition to weakly localizing to mitotic chromosomes in both controls and *traip*$^{-}$ NBs (Fig. 6A,B). The observed FancD2 on chromosome bridges suggests the presence of UFBs and is consistent with a role for Traip in resolving URSCs at mitotic onset.

To understand better the mechanism of URSC and mitotic DNA bridge formation, we used drug treatments to induce replication stress via various mechanisms in control and *traip*$^{-}$ larvae and assayed their survival to adult (Fig. 6C). A major source of URSCs is late-replicating regions, where replication forks fail to converge before mitotic entry (Liu et al., 2014); hydroxyurea increases late-replicating regions by depleting the nucleotide pool and inhibiting replication (Bianchi et al., 1986). Surprisingly, *traip*$^{-}$ mutants were not sensitive to hydroxyurea treatment (Fig. S4A), suggesting that late-replicating region-induced URSCs are not the major target for Traip.

Another source of URSCs is inter-strand crosslinks, which block replication machinery and cause stalled forks; both cisplatin and mitomycin C are inter-strand crosslinking agents (Deans and West, 2011). Whereas controls tolerated high doses of cisplatin and mitomycin C, *traip*$^{-}$ animals only tolerated low doses, with higher doses causing lethality (Fig. 6D), likely due to defects in imaginal disc proliferation (Fig. S4B). The MBs of *traip*$^{-}$ adults raised on cisplatin or mitomycin C were not affected (Fig. S4C,D); however, this may be due to a failure of these drugs to cross the blood brain barrier, as is the case in mammals (Gregg et al., 1992; Reddy and Randerath, 1987). Nonetheless, these experiments indicate that Traip functions to resolve DNA crosslink-induced damage.

TRAIP triggers fork unloading via ubiquitylation of MCM7 (Wu et al., 2019), and therefore requires an intact RING domain for E2-conjugating enzyme binding. Thus, we tested whether the RING domain is required for Traip function in MB development. *GFP::traip*^{L12E,G14D}, which is a control mutant predicted to have a functional RING domain, fully rescued *traip*$^{-}$ MB lobe size (Fig. 6E,F). In contrast, *GFP::traip*^{I8D,A10E}, which is predicted to have a non-functional RING-E2 binding interface, failed to rescue *traip*$^{-}$ MB lobe size (Fig. 6F,G). *GFP::traip*$^{\Delta RING}$ enhanced the *traip*$^{-}$ MB lobe size defect (Fig. 6H), indicating a dominant-negative effect of deleting the RING domain. These results show that *traip* function in MB-NBs is RING dependent, consistent with the known E3 ligase function and role in fork unloading for TRAIP.

Proper MB development requires mitotic but not interphase *traip* localization

We identified for the first time mitotic localization for Traip while characterizing mNG::Traip expression. In interphase, mNG::Traip localized to the nucleus, as previously described (Feng et al., 2016; Harley et al., 2016; Soo Lee et al., 2016). However, during mitosis mNG::Traip became localized to mitotic spindles and concentrated at the centrosomes (Fig. 7A, Movie 5). High-resolution imaging revealed that mNG::Traip forms small puncta that travel poleward along the spindles (Fig. 7B, Movie 6) and also coalesce at the cytokinetic furrow and midbody (Fig. 7C) in late mitosis.

To characterize regions within Traip responsible for its mitotic localization, we expressed GFP::Traip variants in *traip*$^{-}$ CB-NBs via *wor-GAL4*, including full length (FL), RING mutant (I8D, A10E), and several truncations and internal deletions based on the major features of Traip (Fig. S5A). GFP::Traip^{FL} recapitulated the interphase and mitotic localizations of mNG::Traip (Fig. 7D, Fig. S5B). GFP::Traip^{I8D,A10E} localized to the proper sites, but formed aggregates (Fig. S5C). Neither the RING domain nor the first coiled-coil domain was sufficient to mediate any localization (Fig. S5D). Both the second coiled-coil domain and the C-terminal region were sufficient to mediate centrosome localization (Fig. S5E-H). Finally, the C-terminal region was necessary and sufficient for localization to the furrow during mitosis and the nucleus/nucleolus during interphase (Fig. S5G,H). We also tested whether these protein regions are required for Traip MB function, but none was sufficient to rescue *traip*$^{-}$ MB lobe size (Fig. S6A), indicating that Traip function requires multiple domains. Human GFP::TRAIP also failed to rescue *traip*$^{-}$ MB lobe size (Fig. S6A); although the domain structures of Traip and TRAIP are conserved, they are fairly divergent at the protein level (22% identity; Fig. S6B).

We next tested whether mitotic localization of Traip was sufficient for proper MB development. GFP::Traip$^{\Delta NLS}$, which contains a deletion of the nuclear localization signal (NLS), localized similarly to wild-type GFP::Traip during mitosis but was cytoplasmic in interphase (Fig. 7F). Nonetheless, *GFP::traip*$^{\Delta NLS}$ fully rescued *traip*$^{-}$ adult MB lobe size (Fig. 7G,H), 24 h APF MB-NB number (Fig. 7I), KC number (Fig. 7J,K) and nearly completely rescued mitotic chromosome bridging (22/23, Fig. 7L, Movie 7), indicating that Traip function during mitosis is sufficient for MB-NBs. To test whether proper mitotic localization is important for Traip function, we introduced a Tom20 tag to ectopically force Traip to the mitochondria. Tom20::TagRFP::Traip localized cytoplasmically in interphase, and was absent from the spindle region in mitosis (Fig. 7M). Mitochondria-localized Tom20::TagRFP::Traip provided an intermediate rescue of *traip*$^{-}$ MB lobe size (Fig. 7H,N). Given the centrosome and spindle localization and the apparent importance of proper mitotic localization, we hypothesized that *traip*$^{-}$ MB-NBs could have centrosome or spindle defects that could contribute to microcephaly

Development (2022) 149, dev199987. doi:10.1242/dev.199987

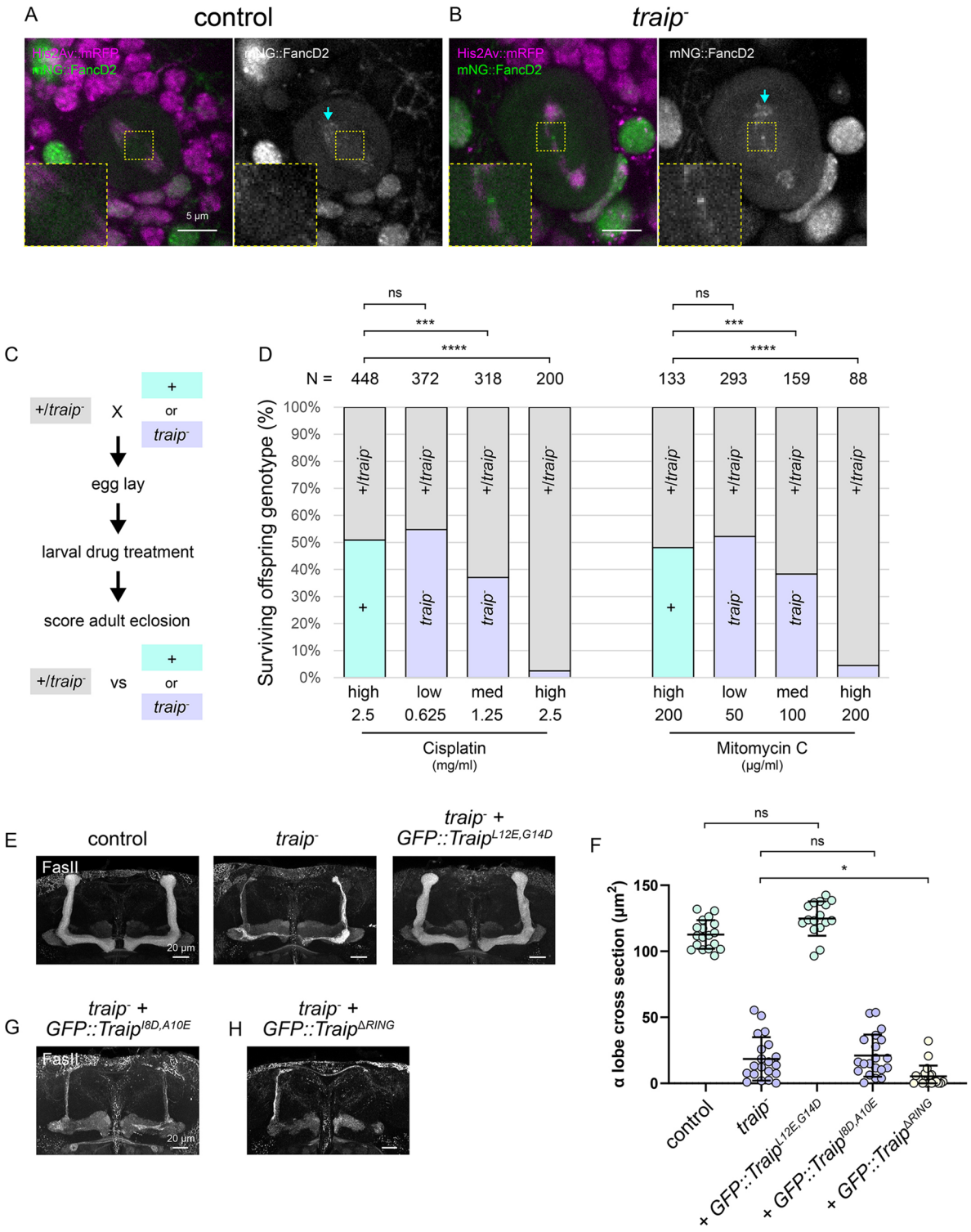

Fig. 6. *traip* suppresses ultrafine bridges and is required for inter-strand crosslink repair. (A,B) Third instar larval CB-NBs expressing mNG::FancD2 (green, gray) with His2Av::mRFP (magenta). 7/12 *traip*$^{-}$ NBs with mitotic DNA bridges had mNG::FancD2 puncta localized on the bridge (B, inset). Both controls and *traip*$^{-}$ have weak localization of mNG::FancD2 on mitotic chromosomes (cyan arrows). Insets show magnifications of the boxed areas. Scale bars: 5 µm. (C) Experimental setup for drug treatment survival assays. +/*traip*$^{-}$ (*traip*^{Exc142}/*CyO*) females were mated to either+(cyan) or *traip*$^{\Delta}$ (purple) males. The females laid eggs for 24 h, which were aged for another 24 h before adding drug. The larvae developed and adult eclosion was scored. Offspring were either +/ *traip*$^{-}$ (+/*traip*$^{\Delta}$) versus+(+/*CyO*) for control crosses (cyan), or +/*traip*$^{-}$ (*traip*$^{\Delta}$/*CyO*) versus *traip*$^{-}$ (*traip*$^{\Delta}$/*traip*^{Exc142}) for *traip*$^{-}$ crosses (purple). (D) Drug treatment survival assay results. Control crosses produced roughly similar numbers of + and +/*traip*$^{-}$ offspring with high doses of inter-strand crosslinking agents cisplatin or mitomycin C. *traip*$^{-}$ crosses also produced similar numbers of *traip*$^{-}$ and +/*traip*$^{-}$ offspring with low doses of either drug, but medium doses were semi-lethal and high doses were almost fully lethal to *traip*$^{-}$ offspring. χ^2 tests were used to determine significance. ns, not significant; ***P<0.001, ****P<0.0001. (E,G,H) MBs stained for FasII. Genotypes are: control, *traip*$^{-}$, *traip*$^{-}$+*GFP::traip*^{L12E,G14D} (E); *traip*$^{-}$+*GFP::traip*^{I8D,A10E} (G); *traip*$^{-}$+*GFP::traip*$^{\Delta RING}$ (H). Transgene expression was driven by *OK107-GAL4*. Scale bars: 20 µm. (F) α lobe cross-section measurements of control, *traip*$^{-}$ and *traip*$^{-}$+*GFP::traip* RING mutant variants. Ordinary one-way ANOVA was used for significance. *P=0.0191. n≥16 MBs/genotype.

Development (2022) 149, dev199987. doi:10.1242/dev.199987

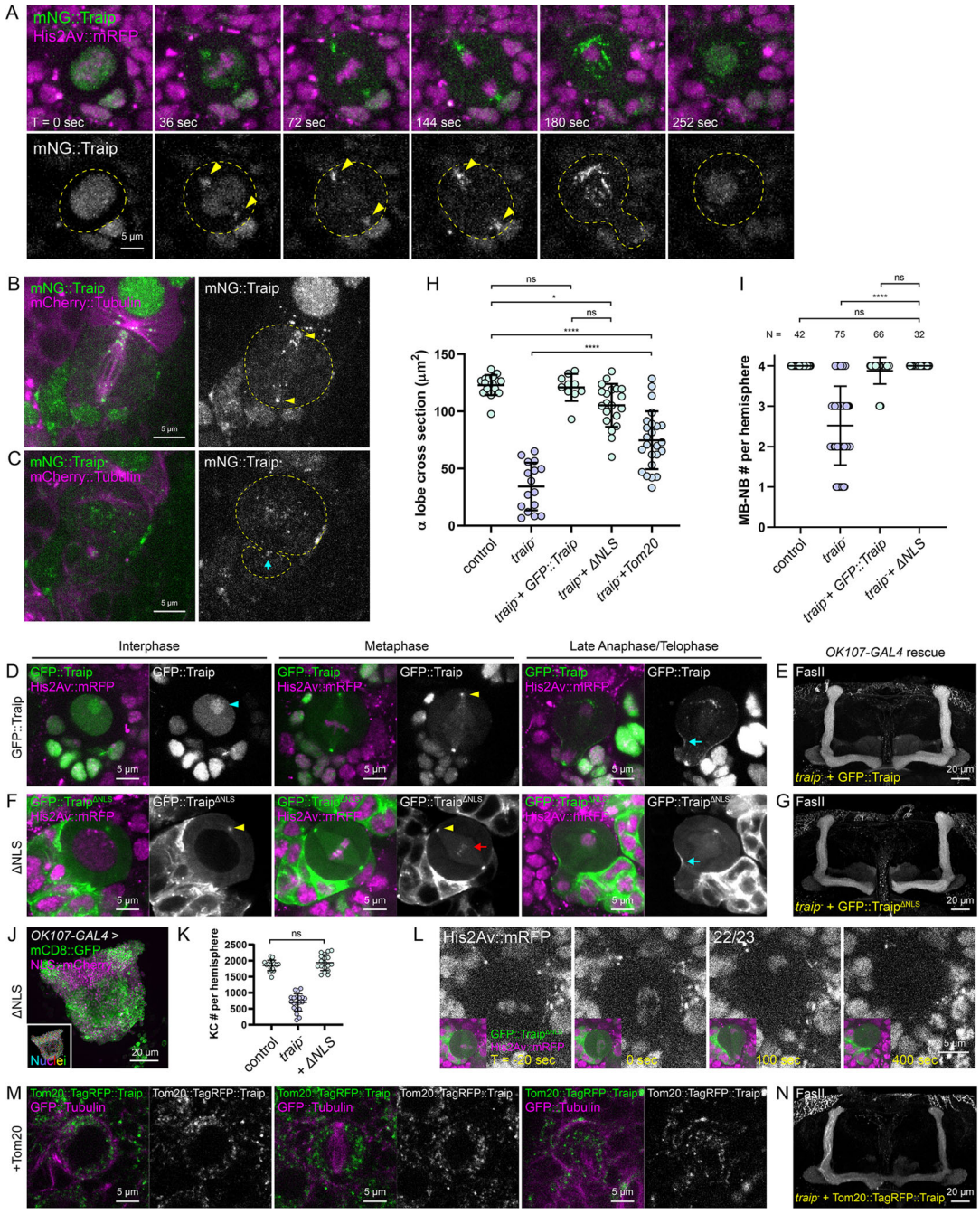

Fig. 7. Traip has a dynamic localization in mitosis. (A) Live imaging of mNG::Traip (green) with His2Av::mRFP (magenta) in third instar larval CB-NB mitosis. At mitotic onset (36 s) mNG::Traip is released from the nucleus and localizes to the centrosomes (yellow arrowheads) and spindle. Yellow dashed lines delineate the NB cell cortex. See also Movie 5. (B,C) High-magnification live imaging of mNG::Traip (green) with *wor-GAL4*>mCherry::Tubulin (magenta). mNG::Traip forms puncta that travel poleward on the spindle and coalesce at the centrosomes (yellow arrowheads, B), and coalesces at the cytokinetic furrow and midbody in late mitosis (cyan arrow, C). See also Movie 6. (D,F) Localization of GFP::Traip variants (green) expressed via *wor-GAL4* with His2Av::mRFP (magenta) in CB-NBs during interphase, metaphase and late mitosis. (D) GFP::Traip^{FL} has nucleolar localization in interphase (cyan arrowhead), centrosome localization in mitosis (yellow arrowhead), and furrow localization in late mitosis (cyan arrow). (F) GFP::Traip$^{\Delta NLS}$ lacks nuclear localization in interphase, but has centrosome localization in interphase and mitosis (yellow arrowheads), furrow localization in late mitosis (cyan arrow), and also localizes to metaphase chromosomes (red arrow). (E,G,N) MBs stained for FasII. Genotypes are: *traip*$^{-}$+*GFP::traip*^{FL} (E); *traip*$^{-}$+*GFP::traip*$^{\Delta NLS}$ (G); and *traip*$^{-}$+*Tom20::TagRFP::traip* (N). Transgene expression was driven by *OK107-GAL4*. (H) α lobe cross-section measurements of control, *traip*$^{-}$, *traip*$^{-}$+*GFP::traip*^{FL}, *traip*$^{-}$+*GFP::traip*$^{\Delta NLS}$ and *traip*$^{-}$+*Tom20::TagRFP::traip*. Ordinary one-way ANOVA was used to determine significance. ns, not significant; *P=0.0448; ****P<0.0001. $n\geq16$ MBs. (I) MB-NB number per hemisphere in 24 h APF control, *traip*$^{-}$, *traip*$^{-}$+*GFP::traip*^{FL} and *traip*$^{-}$+*GFP::traip*$^{\Delta NLS}$ brains. Kruskal–Wallis test was used to determine significance. (J) *OK107-GAL4*>mCD8::GFP (green)+NLS::mCherry (magenta) were used for KC nuclei segmentation and counting (multi-color, inset) of *traip*$^{-}$+*OK107-GAL4>UAS-GFP::traip*$^{\Delta NLS}$. (K) KC numbers are fully rescued in *traip*$^{-}$+*OK107-GAL4>UAS-GFP::traip*$^{\Delta NLS}$. Control and *traip*$^{-}$ reproduced from Fig. 1. $n\geq16$ hemispheres. (L) Live imaging of *traip*$^{-}$+*wor-GAL4*>UAS-GFP::Traip$^{\Delta NLS}$ (green) with His2Av::mRFP (gray, magenta in inset) shows a nearly full rescue of mitotic DNA bridges (22/23). See also Movie 7. (M) Localization of Tom20::TagRFP::Traip (green) with GFP::Tubulin (magenta) in CB-NBs. Tom20::TagRFP fails to localize to the nucleus in interphase, and is absent from the centrosome and spindle region in mitosis. Scale bars: 5 µm (A-D,F,L,M), 20 µm (E,G,J,N).

Development (2022) 149, dev199987. doi:10.1242/dev.199987

phenotypes. However, we detected no abnormalities in centrosome numbers, γ-Tubulin recruitment to centrosomes (Fig. S7A), or in the polarized localization of aPKC (Fig. S7B) in metaphase 24 h APF MB-NBs. Thus, proper mitotic localization of Traip to the spindle, centrosome and/or midbody is important for full Traip function.

DISCUSSION

Our study in *Drosophila* shows that *traip*$^{-}$ shares several characteristics with human microcephaly mutants. First, the *traip*$^{-}$ phenotype is highly brain specific, with body defects being rare. Second, the *traip*$^{-}$ MB phenotype is developmental rather than neurodegenerative, reflecting a primary rather than secondary microcephaly-like disorder. Finally, as with many human microcephaly genes, *traip* functions to promote NPC proliferation and survival. Thus, *traip*$^{-}$ represents a powerful new disease model for understanding the etiological mechanisms underlying microcephaly.

Despite their ubiquitous expression, mutations in microcephaly genes primarily affect the cerebral cortex in humans. Similarly, both *traip* and the DDR microcephaly gene *MCPH1* (Rickmyre et al., 2007) are ubiquitously expressed in *Drosophila*, yet the MB is the only adult structure affected in their mutants. Although many tissues can make up for lost cells via compensatory proliferation (Haynie and Bryant, 1977; Pfau et al., 2016), no such process appears to exist for replacing lost NPCs. Additionally, whereas most NBs have a limited window of proliferation, MB-NBs divide continuously from embryogenesis into late pupal stages (Ito and Hotta, 1992; Truman and Bate, 1988), potentially allowing more accumulation of rare or small effects over many cell cycles. Thus, we speculate that mutations in microcephaly genes likely affect all CB-NBs to some degree, but the MB-NBs are especially sensitive to these mutations as a consequence of their relatively prolonged period of proliferation. We speculate that a similar explanation, including a prolonged period of rapid proliferation and lack of compensatory proliferation, may account for the sensitivity of the human cortex to microcephaly gene mutation.

Our work provides the first link between a known function of Traip and proper brain development. We found that interphase nuclear localization is not required for Traip function, suggesting that Traip interphase functions are dispensable for MB-NB survival under normal conditions. Instead, we discovered the presence of mitotic DNA bridges, sensitivity to inter-strand crosslinking agents, and RING domain dependence, consistent with the well-established role of TRAIP in unloading stalled forks to initiate repair (Fig. 8A; Deng et al., 2019; Priego Moreno et al., 2019; Sonneville et al., 2019). Furthermore, GFP::Traip$^{\Delta NLS}$ rescue experiments suggest either that Traip primarily performs this unloading function during mitosis (Deng et al., 2019), or else that Traip normally functions

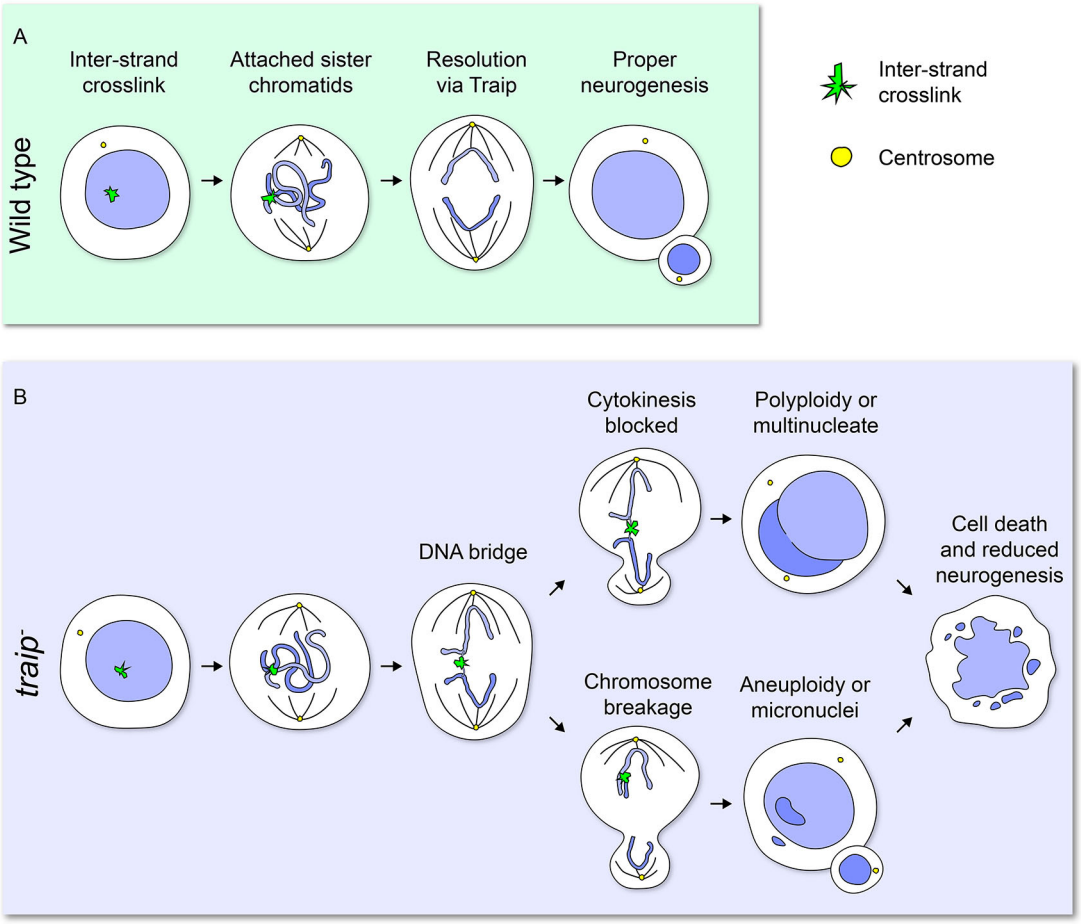

Fig. 8. Model of Traip function in neurogenesis. (A) In wild type, inter-strand crosslinks may prevent completion of DNA replication, resulting in sister chromatids remaining partially attached in mitosis. Traip initiates the resolution of these attached sister chromatids, ensuring chromosome segregation and proper neurogenesis. (B) In *traip*$^{-}$, attached sister chromatids are not properly resolved, leading to DNA bridges in mitosis. DNA bridges could block cytokinesis, leading to formation of polyploid or multinucleated cells (top). Alternatively, DNA bridges could break, leading to formation of aneuploid cells or micronuclei (bottom). These defects could result in cell cycle exit, apoptosis, and ultimately reduced neurogenesis.

Development (2022) 149, dev199987. doi:10.1242/dev.199987

during interphase but is able to unload stalled forks during mitosis if necessary. Alternatively, we cannot rule out the possibility that there may be residual GFP::Traip$^{\Delta NLS}$ in the nucleus that allows continued function during interphase, or else that nuclear localization of Traip is not required for an interphase function. We surmise that *traip*$^{-}$ MB-NBs have stalled replication machinery that remains loaded throughout mitosis, preventing mitotic DNA synthesis repair and proper sister chromatid segregation (Fig. 8B). As anaphase proceeds, attached sister chromatids are pulled to opposite poles and they form UFBs as the under-replicated DNA is stretched out between them. These bridges could be physically broken, leading to chromosome fragmentation, generating aneuploidy or micronuclei and causing nuclear deformations in daughter cells (Gisselsson et al., 2001; Heddle and Carrano, 1977). Alternatively, persistence of DNA bridges at the cytokinetic furrow could induce mitotic exit and furrow regression (Pampalona et al., 2012; Shi and King, 2005), leading to multiple nuclei or polyploidy, which likely prevent further proliferation.

Under normal conditions, MB-NBs are lost at the end of pupal development via caspase-dependent apoptosis (Siegrist et al., 2010). Here, we found that *traip*$^{-}$ MB-NBs are lost prematurely, in part via caspase-dependent cell death, and thus fail to generate proper KC numbers. However, our caspase-inhibition experiments did not fully suppress *traip*$^{-}$ MB phenotypes, suggesting that additional redundant mechanisms may play a role in MB-NB loss. For example, when caspase-dependent apoptosis is inhibited, MB-NBs are primarily lost via autophagy (Pahl et al., 2019). Alternatively, the irregular, crenellated nuclear envelope morphology of some *traip*$^{-}$ MB-NBs (Fig. 5C) could point to non-apoptotic cell death pathways (Kutscher and Shaham, 2017). Finally, aneuploidy-induced cell cycle exit in *traip*$^{-}$ MB-NBs could lead to loss via premature differentiation (Gogendeau et al., 2015). Furthermore, it is likely that loss of KCs and/or GMCs also contributes some to *traip*$^{-}$ MB size defects.

DNA bridge-induced defects likely feed into premature cell loss, but further work is required to dissect the pathways connecting them. In *Drosophila*, polyploid NBs can accumulate significant DNA damage as they enter mitosis (Nano et al., 2019), and chromosome breakage during mitosis in *traip*$^{-}$ could induce death through DNA-damage signaling. *Drosophila* embryos laid by *traip*$^{-}$ mothers do not survive, with extensive chromosome bridging and *Chk2*-dependent cell death, suggesting that DNA damage accumulation leads to cell loss in the rapidly dividing cells of the early embryo (Merkle et al., 2009). In mammalian NPCs, polyploidy and binucleation can cause G1 arrest and apoptosis (Aylon and Oren, 2011; Storchova and Kuffer, 2008). In *Drosophila*, neurons can become polyploid in response to DNA damage (Nandakumar et al., 2020), and NBs can become massively polyploid in some mutants (Poulton et al., 2017; Swider et al., 2019), suggesting that, even though polyploidy may be better tolerated in flies, polyploid NBs are unlikely to complete additional mitoses successfully. We infer the existence of *traip*$^{-}$ aneuploid MB-NBs, which produce a wide range of daughter KC numbers, suggesting that *traip*$^{-}$ generates some aneuploidies that are well tolerated and others that are highly lethal. Similarly, one recent study found that, although many karyotypes are permitted in NBs, loss of both copies of any of the three major *Drosophila* chromosomes resulted in a failure to proliferate and likely elimination (Mirkovic et al., 2019). This parallels the situation in mammals, in which aneuploid NPCs and neurons are common (Rehen et al., 2001), but also sensitive to G1 arrest, cell cycle exit, and apoptosis (Peterson et al., 2012; Storchova and Kuffer, 2008). Thus, both polyploidy and aneuploidy could stop further proliferation in *traip*$^{-}$ MB-NBs by preventing proper mitosis or inducing G1 arrest and cell cycle exit, eventually triggering cell loss via various mechanisms.

In this study, we identified centrosome, spindle and cytokinetic furrow localizations for Traip that are important for function. One possibility is that the dynamic movement of Traip on the mitotic spindle and cytokinetic furrow promotes encounters with unresolved DNA bridges. We never observed GFP::Traip on bridges. However, as a single TRAIP protein is probably sufficient to unload each replisome (Wu et al., 2019), fluorescence detection may be unlikely. Interestingly, centrosome localization is a common aspect of microcephaly-linked proteins, including MCPH1, which also functions in DDR (Jeffers et al., 2008; Rai et al., 2008). Similar to Traip, MCPH1 has mitotic functions required for proper chromosome segregation, and mutations in *MCPH1* lead to lagging chromosomes, DNA bridges and micronuclei (Arroyo et al., 2017; Rickmyre et al., 2007). Mutations in microcephaly genes with centrosome-associated functions, such as *CEP135* and *CDK5RAP2*, cause dysregulation of centrosome numbers, which also lead to chromosome segregation errors and aneuploidy (Barrera et al., 2010; Hussain et al., 2012; Shi et al., 2019). Thus, mitotic roles, ensuring proper chromosome segregation, and suppressing aneuploidy are common features of microcephaly-linked proteins. Future work seeking to understand these shared defects better may reveal a deeper etiological connection across microcephaly disorders.

MATERIALS AND METHODS

Reagents, strains and resources

Details of reagents, strains and resources used are in Table S1.

Drosophila melanogaster

Experimental fly crosses were maintained on Bloomington Recipe Fly food from LabExpress (Ann Arbor, MI, USA) and kept at 25°C. Crosses were either eight virgin females per vial or 20 virgin females per bottle, with at least half as many males. *yw* was used as a control in all genotypes marked '+'. All new transgenic animals were generated using standard embryo injection protocols by BestGene (Chino Hills, CA, USA).

Generation of transgenic *Drosophila*

For *traip*$^{\Delta}$, homology arms were cloned into pUC-attP-3xP3-TR, such that the repair construct contained 1100 bp upstream of the *traip* start codon and 1094 bp downstream of the *traip* stop codon flanking a attP-3xP3-TR replacement. For *mNG::traip*, homology arms and mNeonGreen were cloned into pUC57, such that the repair construct contained 2226 bp upstream of the *traip* start codon, the mNeonGreen coding sequence, and 1093 bp downstream of the *traip* start codon. Guide RNAs were cloned into pU6-chiRNA. Note that PAM sequences in homology arms were mutated such that they were not predicted to be targets for Cas9. Repair template and gRNA plasmid constructs were injected into *y*^{1} *M{RFP[3xP3.PB] GFP[E.3xP3]=vas-Cas9}ZH-2A w*^{1118}*/FM7c* using standard procedures. Putative CRISPR-positive alleles were crossed to *CyO-Cre* to eliminate 3xP3-TagRFP and were fully sequenced from outside the homology arms. *traip*$^{\Delta}$ was further back-crossed to *yw* for three generations and re-sequenced to eliminate a second site lethal mutation. Both CRISPR alleles were crossed to *Df(2R)Exel7153* to test for maternal effect lethality; *traip*$^{\Delta}$ was maternal-effect lethal, and *mNG::traip* was fertile.

traip^{I8D,A10E} and *traip*^{L12E,G14D} were rationally designed using amino acid alignment of Traip and TRAF6, which is a RING domain E3 ligase that has a known crystal structure with its E2-conjugating enzyme Ubc13 (Yin et al., 2009). *traip*$^{\Delta NLS}$ was designed using cNLS Mapper, which predicts importin α-dependent, CDK1-regulated NLS sequences (Kosugi et al., 2009). *traip*^{I8D,A10E}, *traip*^{L12E,G14D} and *traip*$^{\Delta NLS}$ (deletion of positions 357-366 YSIFKKPRLL) were generated using mutagenic primers. *traip*

Development (2022) 149, dev199987. doi:10.1242/dev.199987

truncations were PCR-amplified from cDNA. *traip*, *traip* variants, human *TRAIP* and *FancD2* cDNAs were cloned into pENTR using standard Gateway cloning methods. Gateway cloning was used to move constructs from pENTR into pPGW for *UAS-GFP::traip*^{variants}, pUGW for *ubi-GFP::traip*, pPT20TRW for *UAS-Tom20::TagRFP::traip*, and pUNW for *ubi-mNG::FancD2*.

Drug treatments

Parent flies (*traip*^{Exc142}/*CyO* females and either *yw* or *traip*$^{\Delta}$ males) were crossed for 2-3 days and then transferred to fly food made from 0.6 g of Carolina Formula 4-24 (Fisher Scientific) and 2 ml of ddH_2O. Parents laid eggs for 24 h, eggs were allowed to hatch for 24 h, and then 450 µl of yeast solution (1 g dry yeast sprinkles per 10 ml ddH_2O) with drug was added on top of the food. Drugged larvae were allowed to develop and adults were scored by genotype daily as they eclosed. Concentrated drug stock solutions were reconstituted as follows: Cisplatin at 1 mg/ml in PBS; mitomycin C at 0.5 mg/ml in ddH_2O; hydroxyurea at 5 mg/ml in ddH_2O.

µ-CT

Control, *traip*$^{-}$ and *traip*$^{-}$*+ubi-GFP::traip* flies were processed for µ-CT according to Schoborg et al. (2019). Briefly, adult flies were aged to 2-4 days old, anesthetized on CO_2, de-waxed in PBST (0.5% Triton X-100 in PBS), and fixed in Bouin's solution for 24 h. Fixed flies were washed in 0.1 M Na_2HPO_4 with 1.8% sucrose and then stained in 0.1 N solution of I_2KI for 2 days. Stained flies were washed with ultrapure H_2O and scanned using SkyScan 1172 desktop scanner. Tomograms were generated with NRecon, and 3D volumetric segmentation was performed using Dragonfly. Brain measurements were normalized to thorax width to control for overall size differences among individual flies.

Immunostaining

Animals at appropriate stages were collected and aged: adult flies were aged to 3-4 days old unless otherwise stated; white pre-pupae were collected and aged for 24, 48 or 72 h to obtain pupal stages. Staining procedures were modified from Jenett et al. (2012) and Aso et al. (2014). Tissues were dissected in SF900 S2 cell media (Fisher Scientific) and fixed with 2% paraformaldehyde in SF900 for 2 h at room temperature (RT) or overnight at 4°C. Fixed samples were washed three times in PBST and blocked for 1.5 h in PBST+5% normal goat serum (NGS). Blocked samples were incubated in PBST+NGS with primary antibody for 1-2 h at RT followed by one or two overnight incubations at 4°C. Primary antibody concentrations were as follows: mouse anti-FasII [Developmental Studies Hybridoma Bank (DSHB), 1D4; 1:50]; rat anti-CadN (DSHB, DN-Ex#8; 1:25); mouse anti-Nrg (DSHB, BP104; 1:25); mouse anti-Elav (DSHB, 7E8A 10; 1:100); mouse anti-Lamin (DSHB, ADL84.12; 1:100); mouse anti-Tubulin (DSHB, E7; 1:200); rat anti-DCAD2 (DSHB, DCAD2; 1:20); rabbit anti-γH2Av (Rockland, 600-401-914; 1:100); mouse anti-GFP (Thermo Fisher, A11122; 1:1000); mouse anti-phospho-tyrosine (Millipore, 4G10; 1:100); rabbit anti-phospho-histone H3 (Millipore, H3S10P; 1:40,000); rabbit anti-Dcp-1 (Cell Signaling Technology, 9578; 1:500); mouse anti-γTubulin (Sigma-Aldrich, GTU-88; 1:500); guinea pig anti-Asl (Klebba et al., 2013; 1:20,000); rabbit anti-aPKC (Santa Cruz Biotechnology, C20; 1:1000); guinea pig anti-Dpn (kind gift of J. B. Skeath, Washington University in St Louis, MO, USA; 1:50). Samples were washed five times in PBST+NGS, and then incubated in PBST+NGS with 1:500 secondary antibody (Thermo Fisher, various goat anti-mouse/rabbit/rat/guinea pig secondary antibodies conjugated to Alexa fluor 488/568/647: A11001, A11004, A21235, A21124, A21241, A21242, A11008, A11011, A21244, A11077, A21247 and A21450) and 1× DAPI (Invitrogen, D21490) for 1-2 h at RT followed by one to three overnight incubations at 4°C. Samples were washed three times in PBST+NGS and then three times in PBST, before being post-fixed in 4% paraformaldehyde in PBS for 1 h at RT. Post-fixed samples were washed twice in PBST, and then washed in PBS until all Triton X-100 was removed. Samples were mounted on poly-L-lysine-coated #1.5 coverslips, rinsed in ddH_2O, and then dehydrated through a series of 30%, 50%, 75%, 95% and then three 100% ethanol 10 min baths. Dehydrated coverslips were then bathed three times in 100% xylene for 5 min, before being mounted in DPX on slides with #1.5 coverslips as spacers. DPX was cured at RT overnight. For phalloidin-stained samples, Phalloidin–Atto 647N (Sigma-Aldrich) was added at 1:40 in PBS for 20 min after secondary antibody incubation, and samples were not post-fixed and were mounted in AquaPoly Mount (Polysciences).

Light microscopy

Most fixed samples were imaged using a Zeiss LSM 880 confocal microscope with a 63×/1.4 NA objective, GaAsP detectors, and 405, 488, 561 and 641 nm laser lines, controlled using Zen Black software. Some fixed samples (Figs 4A, 5A,I,J) were imaged using a Nikon W1 spinning disk confocal equipped with a Prime BSI cMOS camera (Photometrics) and a 100×/1.4 NA silicon immersion objective, controlled using Nikon Elements software. Live imaging was performed either using the same Nikon W1 with 100×/1.4 NA silicon or 40×/1.3 NA oil immersion objective, or using an Eclipse Ti2 (Nikon) with a 100×/1.49 NA objective or a 40×/1.3 NA objective and a 1.5× tube lens, an ORCA-Flash 4.0 CMOS camera (Hamamatsu Photonics), and 405, 491, 561 and 642 nm laser lines, controlled by MetaMorph software. For live imaging, larval brains were dissected in Schneider's media and mounted by sandwiching between a #1.5 coverslip and a 50-mm lummox dish, with droplets of Halocarbon oil 700 as a cushion and surrounding the edge of the coverslip.

Image analysis

For MB α lobe cross-sectional analysis, image stacks of α lobes were stack rotated to be perpendicular to the viewing plane using the Interactive Stack Rotation plugin in ImageJ. Rotated MB lobes were then cross-sectioned through the middle of the lobe using the reslice tool, and the area of the resliced MB lobe was measured in ImageJ. For MB volumetric analysis, either FasII-positive or *OK107-GAL4*>mCD8::GFP-positive MB lobes were segmented and measured using the Pixel Classification and 3D Object Analysis tools in Aivia software. For KC counting analysis, the *OK107-GAL4*>NLS::mCherry-positive KCs were similarly segmented and counted using Pixel Classification and 3D Object Analysis tools in Aivia software. For Dcp-1-positive KC normalization, total KCs were estimated via manual counting. γH2Av puncta were thresholded and identified using the 3D Objects Counter in ImageJ. Then, γH2Av objects inside the nucleus, as marked by anti-Lamin immunostaining, were counted in each MB-NB. ImageJ was used to generate maximum intensity projections for presentation.

Statistical analysis

Data analysis was performed using Microsoft Excel and GraphPad Prism. In all graphs, the mean±s.d. and all individual data points are presented. Sample sizes were primarily determined based on the availability of animals of the proper genotype and developmental stage, and the time required for dissection, processing and imaging; given these considerations, we processed 8-12 brains per genotype for most experiments, although some brains were not imaged owing to physical damage. Experiments measuring MB lobe size were typically performed once, with control and *traip*$^{\Delta}$ conditions repeated in each experiment. Shapiro–Wilk test was used to test the assumption of normality. Statistical tests used to determine significance are reported in figure legends.

Acknowledgements

We thank the National Heart, Lung, and Blood Institute Light Microscopy Core, especially Xufeng Wu, for support with confocal microscopy. We thank Bloomington *Drosophila* Stock Center for fly stocks, and Developmental Studies Hybridoma Bank for antibodies. Carey Fagerstrom performed all cloning. Rachel Ng performed the µ-CT experiments. We thank Alex Kelly, Matthew Hannaford and Ramya Varadarajan for helpful discussion, and Todd Schoborg, Brian Galletta, Ed Giniger and Hong Xu for critically reading the manuscript.

Competing interests

The authors declare no competing or financial interests.

Author contributions

Conceptualization: R.S.O.; Formal analysis: R.S.O.; Investigation: R.S.O.; Writing - original draft: R.S.O.; Writing - review & editing: R.S.O., N.M.R.; Visualization: R.S.O.; Supervision: N.M.R.; Funding acquisition: N.M.R.

Funding
This work is supported by the Division of Intramural Research at the National Heart, Lung, and Blood Institute (1ZIAHL006126 to N.M.R.). Deposited in PMC for release after 12 months.

Peer review history
The peer review history is available online at https://journals.biologists.com/dev/article-lookup/doi/10.1242/dev.199987.

References

Abbott, M. K. and Lengyel, J. A. (1991). Embryonic head involution and rotation of male terminalia require the Drosophila locus head involution defective. *Genetics* **129**, 783-789. doi:10.1093/genetics/129.3.783

Arroyo, M., Kuriyama, R., Trimborn, M., Keifenheim, D., Cañuelo, A., Sánchez, A., Clarke, D. J. and Marchal, J. A. (2017). MCPH1, mutated in primary microcephaly, is required for efficient chromosome alignment during mitosis. *Sci. Rep.* **7**, 13019. doi:10.1038/s41598-017-12793-7

Aso, Y., Sitaraman, D., Ichinose, T., Kaun, K. R., Vogt, K., Belliart-Guérin, G., Plaçais, P. Y., Robie, A. A., Yamagata, N., Schnaitmann, C. et al. (2014). Mushroom body output neurons encode valence and guide memory-based action selection in Drosophila. *eLife* **23,** e04580. doi:10.7554/eLife.04580

Aylon, Y. and Oren, M. (2011). p53: guardian of ploidy. *Mol. Oncol.* **5**, 315-323. doi:10.1016/j.molonc.2011.07.007

Barrera, J. A., Kao, L.-R., Hammer, R. E., Seemann, J., Fuchs, J. L. and Megraw, T. L. (2010). CDK5RAP2 regulates centriole engagement and cohesion in mice. *Dev. Cell* **18**, 913-926. doi:10.1016/j.devcel.2010.05.017

Bianchi, V., Pontis, E. and Reichard, P. (1986). Changes of deoxyribonucleoside triphosphate pools induced by hydroxyurea and their relation to DNA synthesis. *J. Biol. Chem.* **261**, 16037-16042. doi:10.1016/S0021-9258(18)66672-4

Bianchi, F. T., Berto, G. E. and Di Cunto, F. (2018). Impact of DNA repair and stability defects on cortical development. *Cell Mol. Life Sci.* **75**, 3963-3976. doi:10.1007/s00018-018-2900-2

Deans, A. J. and West, S. C. (2011). DNA interstrand crosslink repair and cancer. *Nat. Rev. Cancer* **11**, 467-480. doi:10.1038/nrc3088

Deng, L., Wu, R. A., Sonneville, R., Kochenova, O. V., Labib, K., Pellman, D. and Walter, J. C. (2019). Mitotic CDK promotes replisome disassembly, fork breakage, and complex DNA rearrangements. *Mol. Cell* **73**, 915-929.e6. doi:10.1016/j.molcel.2018.12.021

Feng, W., Guo, Y., Huang, J., Deng, Y., Zang, J. and Huen, M. S.-Y. (2016). TRAIP regulates replication fork recovery and progression via PCNA. *Cell Discov.* **2**, 16016. doi:10.1038/celldisc.2016.16

Gisselsson, D., Björk, J., Höglund, M., Mertens, F., Dal Cin, P., Åkerman, M. and Mandahl, N. (2001). Abnormal nuclear shape in solid tumors reflects mitotic instability. *Am. J. Pathol.* **158**, 199-206. doi:10.1016/S0002-9440(10)63958-2

Gogendeau, D., Siudeja, K., Gambarotto, D., Pennetier, C., Bardin, A. J. and Basto, R. (2015). Aneuploidy causes premature differentiation of neural and intestinal stem cells. *Nat. Commun.* **6**, 8894. doi:10.1038/ncomms9894

Gregg, R. W., Molepo, J. M., Monpetit, V. J., Mikael, N. Z., Redmond, D., Gadia, M. and Stewart, D. J. (1992). Cisplatin neurotoxicity: the relationship between dosage, time, and platinum concentration in neurologic tissues, and morphologic evidence of toxicity. *J. Clin. Oncol.* **10**, 795-803. doi:10.1200/JCO.1992.10.5.795

Han, Y. G., Yun, M., Choi, M., Lee, S.-G. and Kim, H. (2019). TRAIP regulates Histone H2B monoubiquitination in DNA damage response pathways. *Oncol. Rep.* **41**, 3305-3312. doi:10.3892/or.2019.7092

Harley, M. E., Murina, O., Leitch, A., Higgs, M. R., Bicknell, L. S., Yigit, G., Blackford, A. N., Zlatanou, A., Mackenzie, K. J., Reddy, K. et al. (2016). TRAIP promotes DNA damage response during genome replication and is mutated in primordial dwarfism. *Nat. Genet.* **48**, 36-43. doi:10.1038/ng.3451

Haynie, J. L. and Bryant, P. J. (1977). The effects of X-rays on the proliferation dynamics of cells in the imaginal wing disc of Drosophila melanogaster. *Wilhelm Roux'. Archiv.* **183**, 85-100. doi:10.1007/BF00848779

Heddle, J. A. and Carrano, A. V. (1977). The DNA content of micronuclei induced in mouse bone marrow by γ-irradiation: evidence that micronuclei arise from acentric chromosomal fragments. *Mutat. Res.* **44**, 63-69. doi:10.1016/0027-5107(77)90115-4

Heisenberg, M. (2003). Mushroom body memoir: from maps to models. *Nat. Rev. Neurosci.* **4**, 266-275. doi:10.1038/nrn1074

Heisenberg, M., Heusipp, M. and Wanke, C. (1995). Structural plasticity in the Drosophila brain. *J. Neurosci.* **15**, 1951-1960. doi:10.1523/JNEUROSCI.15-03-01951.1995

Hoffmann, S., Smedegaard, S., Nakamura, K., Mortuza, G. B., Räschle, M., Ibañez de Opakua, A., Oka, Y., Feng, Y., Blanco, F. J., Mann, M. et al. (2016). TRAIP is a PCNA-binding ubiquitin ligase that protects genome stability after replication stress. *J. Cell Biol.* **212**, 63-75. doi:10.1083/jcb.201506071

Hussain, M. S., Baig, S. M., Neumann, S., Nürnberg, G., Farooq, M., Ahmad, I., Alef, T., Hennies, H. C., Technau, M., Altmüller, J. et al. (2012). A truncating mutation of CEP135 causes primary microcephaly and disturbed centrosomal function. *Am. J. Hum. Genet.* **90**, 871-878. doi:10.1016/j.ajhg.2012.03.016

Ito, K. and Hotta, Y. (1992). Proliferation pattern of postembryonic neuroblasts in the brain of Drosophila melanogaster. *Dev. Biol.* **149**, 134-148. doi:10.1016/0012-1606(92)90270-Q

Jayaraman, D., Bae, B.-I. and Walsh, C. A. (2018). The genetics of primary microcephaly. *Annu. Rev. Genomics. Hum. Genet.* **19**, 177-200. doi:10.1146/annurev-genom-083117-021441

Jeffers, L. J., Coull, B. J., Stack, S. J. and Morrison, C. G. (2008). Distinct BRCT domains in Mcph1/Brit1 mediate ionizing radiation-induced focus formation and centrosomal localization. *Oncogene* **27**, 139-144. doi:10.1038/sj.onc.1210595

Jenett, A., Rubin, G. M., Ngo, T. T., Shepherd, D., Murphy, C., Dionne, H., Pfeiffer, B. D., Cavallaro, A., Hall, D., Jeter, J. et al. (2012). A GAL4-driver line resource for Drosophila neurobiology. *Cell Rep.* **2**, 991-1001. doi:10.1016/j.celrep.2012.09.011

Khetarpal, P., Das, S., Panigrahi, I. and Munshi, A. (2016). Primordial dwarfism: overview of clinical and genetic aspects. *Mol. Genet. Genomics* **291**, 1-15. doi:10.1007/s00438-015-1110-y

Klebba, J. E., Buster, D. W., Nguyen, A. L., Swatkoski, S., Gucek, M., Rusan, N. M. and Rogers, G. C. (2013). Polo-like kinase 4 autodestructs by generating its Slimb-binding phosphodegron. *Curr. Biol.* **23**, 2255-2261. doi:10.1016/j.cub.2013.09.019

Kosugi, S., Hasebe, M., Tomita, M. and Yanagawa, H. (2009). Systematic identification of cell cycle-dependent yeast nucleocytoplasmic shuttling proteins by prediction of composite motifs. *Proc. Natl. Acad. Sci. USA* **106**, 10171-10176. doi:10.1073/pnas.0900604106

Kutscher, L. M. and Shaham, S. (2017). Non-apoptotic cell death in animal development. *Cell Death Differ.* **24**, 1326-1336. doi:10.1038/cdd.2017.20

Larsen, N. B., Gao, A. O., Sparks, J. L., Gallina, I., Wu, R. A., Mann, M., Räschle, M., Walter, J. C. and Duxin, J. P. (2019). Replication-coupled DNA-protein crosslink repair by SPRTN and the proteasome in Xenopus egg extracts. *Mol. Cell* **73**, 574-588.e7. doi:10.1016/j.molcel.2018.11.024

Lee, T., Lee, A. and Luo, L. (1999). Development of the Drosophila mushroom bodies: sequential generation of three distinct types of neurons from a neuroblast. *Development* **126**, 4065-4076. doi:10.1242/dev.126.18.4065

Liu, Y., Nielsen, C. F., Yao, Q. and Hickson, I. D. (2014). The origins and processing of ultra fine anaphase DNA bridges. *Curr. Opin. Genet. Dev.* **26**, 1-5. doi:10.1016/j.gde.2014.03.003

Merkle, J. A., Rickmyre, J. L., Garg, A., Loggins, E. B., Jodoin, J. N., Lee, E., Wu, L. P. and Lee, L. A. (2009). no poles encodes a predicted E3 ubiquitin ligase required for early embryonic development of Drosophila. *Development* **136**, 449-459. doi:10.1242/dev.027599

Mirkovic, M., Guilgur, L. G., Tavares, A., Passagem-Santos, D. and Oliveira, R. A. (2019). Induced aneuploidy in neural stem cells triggers a delayed stress response and impairs adult life span in flies. *PLoS Biol.* **17**, e3000016. doi:10.1371/journal.pbio.3000016

Modi, M. N., Shuai, Y. and Turner, G. C. (2020). The drosophila mushroom body: from architecture to algorithm in a learning circuit. *Annu. Rev. Neurosci.* **43**, 465-484. doi:10.1146/annurev-neuro-080317-0621333

Naim, V. and Rosselli, F. (2009). The FANC pathway and BLM collaborate during mitosis to prevent micro-nucleation and chromosome abnormalities. *Nat. Cell Biol.* **11**, 761-768. doi:10.1038/ncb1883

Nandakumar, S., Grushko, O. and Buttitta, L. A. (2020). Polyploidy in the adult Drosophila brain. *eLife* **9**, e54385. doi:10.7554/eLife.54385

Nano, M. and Basto, R. (2017). Consequences of centrosome dysfunction during brain development. *Adv. Exp. Med. Biol.* **1002**, 19-45. doi:10.1007/978-3-319-57127-0_2

Nano, M., Gemble, S., Simon, A., Pennetier, C., Fraisier, V., Marthiens, V. and Basto, R. (2019). Cell-cycle asynchrony generates DNA damage at mitotic entry in polyploid cells. *Curr. Biol.* **29**, 3937-3945.e7. doi:10.1016/j.cub.2019.09.041

Pahl, M. C., Doyle, S. E. and Siegrist, S. E. (2019). E93 integrates neuroblast intrinsic state with developmental time to terminate MB neurogenesis via autophagy. *Curr. Biol.* **29**, 750-762.e3. doi:10.1016/j.cub.2019.01.039

Pampalona, J., Frías, C., Genescà, A. and Tusell, L. (2012). Progressive telomere dysfunction causes cytokinesis failure and leads to the accumulation of polyploid cells. *PLoS Genet.* **8**, e1002679. doi:10.1371/journal.pgen.1002679

Park, E.-S., Choi, S., Kim, J.-M., Jeong, Y., Choe, J., Park, C.-S., Choi, Y. and Rho, J. (2007). Early embryonic lethality caused by targeted disruption of the TRAF-interacting protein (TRIP) gene. *Biochem. Biophys. Res. Commun.* **363**, 971-977. doi:10.1016/j.bbrc.2007.09.103

Parks, A. L., Cook, K. R., Belvin, M., Dompe, N. A., Fawcett, R., Huppert, K., Tan, L. R., Winter, C. G., Bogart, K. P., Deal, J. E. et al. (2004). Systematic generation of high-resolution deletion coverage of the Drosophila melanogaster genome. *Nat. Genet.* **36**, 288-292. doi:10.1038/ng1312

Passemard, S., Kaindl, A. M. and Verloes, A. (2013). Microcephaly. *Handb. Clin. Neurol.* **111**, 129-141. doi:10.1016/B978-0-444-52891-9.00013-0

Peterson, S. E., Yang, A. H., Bushman, D. M., Westra, J. W., Yung, Y. C., Barral, S., Mutoh, T., Rehen, S. K. and Chun, J. (2012). Aneuploid cells are differentially susceptible to caspase-mediated death during embryonic cerebral cortical development. *J. Neurosci.* **32**, 16213-16222. doi:10.1523/JNEUROSCI.3706-12.2012

Pfau, S. J., Silberman, R. E., Knouse, K. A. and Amon, A. (2016). Aneuploidy impairs hematopoietic stem cell fitness and is selected against in regenerating tissues in vivo. *Genes Dev.* **30**, 1395-1408. doi:10.1101/gad.278820.116

Poulton, J. S., Cuningham, J. C. and Peifer, M. (2017). Centrosome and spindle assembly checkpoint loss leads to neural apoptosis and reduced brain size. *J. Cell Biol.* **216**, 1255-1265. doi:10.1083/jcb.201607022

Priego Moreno, S., Jones, R. M., Poovathumkadavil, D., Scaramuzza, S. and Gambus, A. (2019). Mitotic replisome disassembly depends on TRAIP ubiquitin ligase activity. *Life Sci. Alliance* **2**, e201900390. doi:10.26508/lsa.201900390

Rai, R., Phadnis, A., Haralkar, S., Badwe, R. A., Dai, H., Li, K. and Lin, S.-Y. (2008). Differential regulation of centrosome integrity by DNA damage response proteins. *Cell Cycle* **7**, 2225-2233. doi:10.4161/cc.7.14.6303

Reddy, M. V. and Randerath, K. (1987). 32P-analysis of DNA adducts in somatic and reproductive tissues of rats treated with the anticancer antibiotic, mitomycin C. *Mutat. Res.* **179**, 75-88. doi:10.1016/0027-5107(87)90043-1

Rehen, S. K., McConnell, M. J., Kaushal, D., Kingsbury, M. A., Yang, A. H. and Chun, J. (2001). Chromosomal variation in neurons of the developing and adult mammalian nervous system. *Proc. Natl. Acad. Sci. USA* **98**, 13361-13366. doi:10.1073/pnas.231487398

Rickmyre, J. L., Dasgupta, S., Ooi, D. L.-Y., Keel, J., Lee, E., Kirschner, M. W., Waddell, S. and Lee, L. A. (2007). The Drosophila homolog of MCPH1, a human microcephaly gene, is required for genomic stability in the early embryo. *J. Cell Sci.* **120**, 3565-3577. doi:10.1242/jcs.016626

Royou, A., Gagou, M. E., Karess, R. and Sullivan, W. (2010). BubR1- and Polo-coated DNA tethers facilitate poleward segregation of acentric chromatids. *Cell* **140**, 235-245. doi:10.1016/j.cell.2009.12.043

Schoborg, T. A., Smith, S. L., Smith, L. N., Morris, H. D. and Rusan, N. M. (2019). Micro-computed tomography as a platform for exploring Drosophila development. *Development* **146**, dev176685. doi:10.1242/dev.176685

Shi, Q. and King, R. W. (2005). Chromosome nondisjunction yields tetraploid rather than aneuploid cells in human cell lines. *Nature* **437**, 1038-1042. doi:10.1038/nature03958

Shi, L., Qalieh, A., Lam, M. M., Keil, J. M. and Kwan, K. Y. (2019). Robust elimination of genome-damaged cells safeguards against brain somatic aneuploidy following Knl1 deletion. *Nat. Commun.* **10**, 2588. doi:10.1038/s41467-019-10411-w

Siegrist, S. E., Haque, N. S., Chen, C.-H., Hay, B. A. and Hariharan, I. K. (2010). Inactivation of both Foxo and reaper promotes long-term adult neurogenesis in Drosophila. *Curr. Biol.* **20**, 643-648. doi:10.1016/j.cub.2010.01.060

Sonneville, R., Bhowmick, R., Hoffmann, S., Mailand, N., Hickson, I. D. and Labib, K. (2019). TRAIP drives replisome disassembly and mitotic DNA repair synthesis at sites of incomplete DNA replication. *eLife* **8**, e48686. doi:10.7554/eLife.48686

Soo Lee, N., Jin Chung, H., Kim, H.-J., Yun Lee, S., Ji, J.-H., Seo, Y., Hun Han, S., Choi, M., Yun, M., Lee, S.-G. et al. (2016). TRAIP/RNF206 is required for recruitment of RAP80 to sites of DNA damage. *Nat. Commun.* **7**, 10463. doi:10.1038/ncomms10463

Storchova, Z. and Kuffer, C. (2008). The consequences of tetraploidy and aneuploidy. *J. Cell Sci.* **121**, 3859-3866. doi:10.1242/jcs.039537

Swider, Z. T., Ng, R. K., Varadarajan, R., Fagerstrom, C. J. and Rusan, N. M. (2019). Fascetto (PRC1) interacting protein (FIP) ensures proper cytokinesis and ploidy. *Mol. Biol. Cell* **30**, 992-1007. doi:10.1091/mbc.E18-09-0573

Truman, J. W. and Bate, M. (1988). Spatial and temporal patterns of neurogenesis in the central nervous system of Drosophila melanogaster. *Dev. Biol.* **125**, 145-157. doi:10.1016/0012-1606(88)90067-X

Villa, F., Fujisawa, R., Ainsworth, J., Nishimura, K., Lie-A-Ling, M., Lacaud, G. and Labib, K. P. M. (2021). CUL2LRR1, TRAIP and p97 control CMG helicase disassembly in the mammalian cell cycle. *EMBO Rep.* **22**, e52164. doi:10.15252/embr.202052164

Wu, R. A., Semlow, D. R., Kamimae-Lanning, A. N., Kochenova, O. V., Chistol, G., Hodskinson, M. R., Amunugama, R., Sparks, J. L., Wang, M., Deng, L. et al. (2019). TRAIP is a master regulator of DNA interstrand crosslink repair. *Nature* **567**, 267-272. doi:10.1038/s41586-019-1002-0

Wu, R. A., Pellman, D. S. and Walter, J. C. (2020). The ubiquitin ligase TRAIP: double-edged sword at the replisome. *Trends Cell Biol.* **31**, 75-85. doi:10.1016/j.tcb.2020.11.007

Yin, Q., Lin, S. C., Lamothe, B., Lu, M., Lo, Y. C., Hura, G., Zheng, L., Rich, R. L., Campos, A. D. and Myszka, D. G. et al. (2009). E2 interaction and dimerization in the crystal structure of TRAF6. *Nat. Struct. Mol. Biol.* **16**, 658-666. doi:10.1038/nsmb.1605